



# Toward a minimal representation of aerosols in climate models: description and evaluation in the Community Atmosphere Model CAM5

X. Liu<sup>1</sup>, R. C. Easter<sup>1</sup>, S. J. Ghan<sup>1</sup>, R. Zaveri<sup>1</sup>, P. Rasch<sup>1</sup>, X. Shi<sup>1</sup>, J.-F. Lamarque<sup>2</sup>, A. Gettelman<sup>2</sup>, H. Morrison<sup>2</sup>, F. Vitt<sup>2</sup>, A. Conley<sup>2</sup>, S. Park<sup>2</sup>, R. Neale<sup>2</sup>, C. Hannay<sup>2</sup>, A. M. L. Ekman<sup>3</sup>, P. Hess<sup>4</sup>, N. Mahowald<sup>5</sup>, W. Collins<sup>6</sup>, M. J. Iacono<sup>7</sup>, C. S. Bretherton<sup>8</sup>, M. G. Flanner<sup>9</sup>, and D. Mitchell<sup>10</sup>

<sup>1</sup>Atmospheric Science and Global Change Division, Pacific Northwest National Laboratory, Richland, Washington, USA

<sup>2</sup>National Center for Atmospheric Research, Boulder, Colorado, USA

<sup>3</sup>Department of Meteorology and Bert Bolin Centre for Climate Research, Stockholm University, Sweden

<sup>4</sup>Biological and Environmental Engineering, Cornell University, Ithaca, New York, USA

<sup>5</sup>Earth and Atmospheric Sciences, Cornell University, Ithaca, New York, USA

<sup>6</sup>Earth Sciences Division, Lawrence Berkeley National Laboratory, Berkeley, California, USA

<sup>7</sup>Atmospheric and Environmental Research, Inc., Lexington, Massachusetts, USA

<sup>8</sup>Department of Atmospheric Sciences, University of Washington, Seattle, Washington, USA

<sup>9</sup>Department of Atmospheric, Oceanic & Space Sciences, Univ. of Michigan, 2455 Hayward St., Ann Arbor, Michigan, USA

<sup>10</sup>Division of Atmospheric Sciences, Desert Research Institute, Reno, Nevada, USA

*Correspondence to:* X. Liu (xiaohong.liu@pnnl.gov)

Received: 26 October 2011 – Published in Geosci. Model Dev. Discuss.: 12 December 2011

Revised: 9 April 2012 – Accepted: 13 April 2012 – Published: 21 May 2012

**Abstract.** A modal aerosol module (MAM) has been developed for the Community Atmosphere Model version 5 (CAM5), the atmospheric component of the Community Earth System Model version 1 (CESM1). MAM is capable of simulating the aerosol size distribution and both internal and external mixing between aerosol components, treating numerous complicated aerosol processes and aerosol physical, chemical and optical properties in a physically-based manner. Two MAM versions were developed: a more complete version with seven lognormal modes (MAM7), and a version with three lognormal modes (MAM3) for the purpose of long-term (decades to centuries) simulations. In this paper a description and evaluation of the aerosol module and its two representations are provided. Sensitivity of the aerosol lifecycle to simplifications in the representation of aerosol is discussed.

Simulated sulfate and secondary organic aerosol (SOA) mass concentrations are remarkably similar between MAM3 and MAM7. Differences in primary organic matter (POM) and black carbon (BC) concentrations between MAM3 and MAM7 are also small (mostly within 10%). The mineral dust

global burden differs by 10% and sea salt burden by 30–40% between MAM3 and MAM7, mainly due to the different size ranges for dust and sea salt modes and different standard deviations of the log-normal size distribution for sea salt modes between MAM3 and MAM7. The model is able to qualitatively capture the observed geographical and temporal variations of aerosol mass and number concentrations, size distributions, and aerosol optical properties. However, there are noticeable biases; e.g., simulated BC concentrations are significantly lower than measurements in the Arctic. There is a low bias in modeled aerosol optical depth on the global scale, especially in the developing countries. These biases in aerosol simulations clearly indicate the need for improvements of aerosol processes (e.g., emission fluxes of anthropogenic aerosols and precursor gases in developing countries, boundary layer nucleation) and properties (e.g., primary aerosol emission size, POM hygroscopicity). In addition, the critical role of cloud properties (e.g., liquid water content, cloud fraction) responsible for the wet scavenging of aerosol is highlighted.

## 1 Introduction

Atmospheric aerosol is recognized as one of the most important forcing agents in the climate system (Forster et al., 2007). Aerosol influences the Earth's radiative balance by directly scattering and absorbing solar and terrestrial radiation (direct effect). Aerosol affects the climate system indirectly by acting as cloud condensation nuclei (CCN) and ice nuclei (IN) and changing cloud microphysical and radiative properties (indirect effect). Aerosol can change cloud cover by heating the atmosphere in which clouds reside (semi-direct effect), and reduce the snow and land and sea ice albedos by deposition and melting of snow and ice (cryosphere radiative effect) (Flanner et al., 2007). After decades of intensive studies, aerosol forcings are still one of the largest uncertainties in projecting future climate change (Forster et al., 2007; Stevens and Feingold, 2009).

Recognizing the importance of aerosol in the climate system, almost all global climate models (GCMs) have implemented treatments of aerosol and its influence on climate. Unlike most greenhouse gases, which due to their long lifetimes ( $\sim 5\text{--}10^2$  yr) have a relatively uniform spatial distribution, aerosol particles have short lifetimes ( $\sim$ days) and hence large spatial variations. In addition, aerosol particles span a spectrum of size ranges ( $10^{-3}$  to  $10^1$   $\mu\text{m}$ ), multiple chemical species (e.g., sulfate, black carbon (BC), organic matter (OM), mineral dust and sea salt), and change through complicated physical and chemical aging in the atmosphere. This diversity and complexity imposes a great challenge to representing aerosol processes and properties in GCMs.

There are several methods of aerosol treatments in GCMs. The bulk method only predicts mass mixing ratio of various aerosol species and prescribes fixed aerosol size distributions in order to convert aerosol mass to number mixing ratio. External mixing is often assumed between different aerosol species (each particle is composed of only one chemical species), and a time scale of 1–2 days is prescribed for the aging of carbonaceous aerosols from hydrophobic to hydrophilic state. The bulk method neglects the temporal and spatial variations of the aerosol size distribution. It also neglects the fact that different aerosol species are usually internally mixed (Clarke et al., 2004; Moffet and Prather, 2009), which for BC and sulfate can enhance absorption of sunlight by up to a factor of two (Jacobson, 2003). Neglecting this internal mixture can significantly affect estimates of aerosol direct forcing (Jacobson, 2001).

The most sophisticated and accurate method for aerosol treatment in GCMs is the sectional method (Jacobson, 2001; Adams and Seinfeld, 2002; Spracklen et al., 2005) when using a sufficient number of size bins. However, it is still prohibitive for GCMs to use this method for long simulations (decades to centuries) due to limited computational resources. An intermediate treatment is the modal method (e.g., Whitby and McMurry, 1997; Wilson et al., 2001; Herzog et al., 2004; Vignati et al., 2004; Easter et al., 2004), in which

aerosol size distributions are represented by multiple log-normal functions. By predicting mass mixing ratios of different aerosol species and number mixing ratio within each mode and prescribing standard deviations of log-normal size distributions based on observations, aerosol size distributions can be derived. The modal method generally assumes that different aerosol species are internally mixed within modes and externally mixed among modes, and thus represents aerosol mixing states more realistically than the bulk method. The modal method has been implemented in many climate models, e.g., ECHAM5 (Stier et al., 2005), Community Atmosphere Model version 2 (CAM2) (Ghan and Easter, 2006) and version 3 (CAM3) (Wang et al., 2009). The quadrature method of moments (QMOM) (McGraw, 1997; Wright et al., 2001; Yoon and McGraw, 2004) has some similarities to the modal method, but is more powerful in that it does not require assumptions about the shape of the aerosol size distribution (e.g., log-normal). Another important consideration is the number of mixing state categories (or “types”) that are used to represent the aerosol mixing state. In most of the models that do treat mixing state, just a few mixing state categories are used in each size range (e.g., fresh/hydrophobic and aged/mixed/hygroscopic in the sub-micron range, and dust and sea salt in the super-micron) (Aquila et al., 2011; Seland et al., 2008; Wang et al., 2009), but a few studies have used many more categories (Jacobson, 2001; Bauer et al., 2008).

Numerous processes in the atmosphere affect aerosol physical, chemical and optical properties (e.g., number/mass concentration, size, density, shape, refractive index, chemical composition): aerosol nucleation, coagulation, condensational growth, gas- and aqueous-phase chemistry, emission, dry deposition and gravitational settling, water uptake, in-cloud and below-cloud scavenging, and release from evaporated cloud and rain droplets. Uncertainties in the treatment of these processes in GCMs will influence our confidence in estimates of aerosol radiative forcing and climate impacts. For example, wet removal of aerosol was identified as one of the major processes responsible for the large differences (by more than a factor of 10) in aerosol concentrations in the free troposphere and in the polar regions among models participating in the Aerosol Model Intercomparison Initiative (AeroCom) project (Textor et al., 2006; Koch et al., 2009). There are still large uncertainties in secondary organic aerosol (SOA) formation and aging and its physical and chemical properties (Kanakidou et al., 2005; Farina et al., 2010; Jimenez et al., 2009). Large uncertainties exist for aerosol emissions, including emission sizes, injection heights of biomass burning aerosol, and flux rates of sea salt and mineral dust. The uncertainty in aerosol mixing states will impact its hygroscopicity, water uptake, droplet activation, and optical properties important for aerosol direct and indirect radiative forcing.

The modal method is a favorable approach for conserving computational resources and for representing aerosol size

distributions and mixing states with sufficient accuracy to estimate aerosol radiative forcing. However, even for models adopting this method, there can be large differences among models in selecting the number of modes and the number of aerosol species in each mode. The treatment of aerosol aging, water uptake, SOA formation and optics of aerosol internal/external mixtures can be different. However, for GCMs with many detailed and time-consuming components (atmosphere, land, ocean, sea ice, biosphere with carbon/nitrogen cycles) for long simulations (decades to centuries), a minimal representation of aerosol that can capture the essentials of aerosol forcing on climate is highly desirable.

In this study we have implemented a plausible set of aerosol lifecycle processes in the Community Atmospheric Model version 5 (CAM5). Two versions of the aerosol module are developed, including one relatively complete and one simplified representation of the aerosol. The goal of this paper is to provide a description and evaluation of the aerosol module with its two representations. Sensitivity of the aerosol lifecycle to simplifications in the representation of aerosol is discussed. The impact of simplifications on aerosol forcing and the decomposition of the total anthropogenic aerosol forcing by mechanism and species is presented in a companion paper (Ghan et al., 2012). Section 2 introduces the model used, including both representations of the aerosol. Section 3 compares global distributions and budgets of aerosol simulated with both representations. Section 4 evaluates simulations with both representations of the aerosol. Section 5 considers some sensitivity experiments to improve understanding of the differences found for the two representations. Conclusions and future work are summarized in Sect. 6.

## 2 Model description

The model used in this study is version 5.1 of the Community Atmosphere Model (CAM5.1), which is a major update of CAM3.5 described by Gent et al. (2009). With the exception of deep cumulus convection, almost all processes in CAM5.1 differ markedly from CAM3.5. In this section, we introduce the treatment of aerosols in CAM5. The details of aerosol and other physical processes (clouds, radiation, and turbulence) are given in Sects. S1.1–1.5 of the Supplement of this paper.

We have implemented two different modal representations of the aerosol. A 7-mode version of the modal aerosol model (MAM7) serves as a benchmark for further simplification. It includes Aitken, accumulation, primary carbon, fine dust and sea salt, and coarse dust and sea salt modes (Fig. 1). Within a single mode (for example, the accumulation mode) we predict the mass mixing ratios of internally-mixed sulfate ( $\text{SO}_4$ ), ammonium ( $\text{NH}_4$ ), SOA, primary organic matter (POM) and BC aged from the primary carbon mode, sea salt, and the number mixing ratio of accumulation mode particles. POM and BC are emitted to the primary carbon mode,

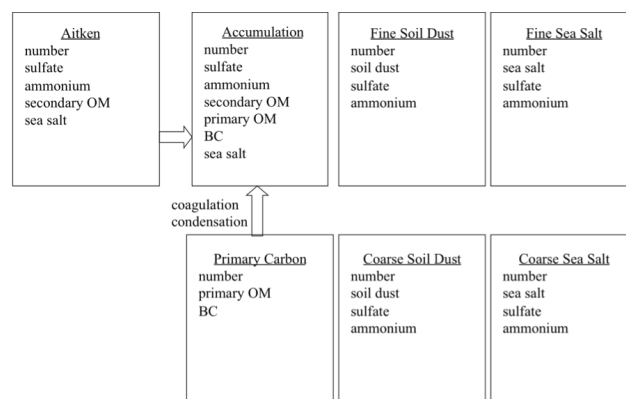


**Fig. 1.** Predicted species for interstitial and cloud-borne component of each aerosol mode in MAM7.

then are aged and transferred to the accumulation mode by condensation of  $\text{H}_2\text{SO}_4$ ,  $\text{NH}_3$  and semi-volatile organics and by coagulation with Aitken and accumulation modes (see Sects. S1.1.5 and S1.1.6 in the Supplement).

Aerosol particles (AP) exist in different attachment states. We mostly think of AP that are suspended in air (either clear or cloudy air), and these are referred to as interstitial AP. AP can also be attached to (or contained within) different hydrometeors, such as cloud droplets. In CAM5, the AP in stratiform cloud droplets (referred to as stratiform cloud-borne AP) are explicitly predicted, as in Easter et al. (2004). The AP in convective cloud droplets are not treated explicitly. Rather, they are lumped with the interstitial AP in the model, and they are diagnosed from the “lumped interstitial + convective cloud-borne” amount when needed. The lumped interstitial AP species are transported in three dimensions. The stratiform cloud-borne AP species are not transported (except by vertical turbulent mixing) but are saved every time step, which saves computer time but has little impact on their predicted values (Ghan and Easter, 2006).

The size distributions of each mode are assumed to be log-normal, with the mode dry or wet radius varying as number and total dry or wet volume change. The geometric standard deviation ( $\sigma_g$ ) of each mode is prescribed (Easter et al., 2004 and references therein) and given in Table 1, along with the typical size range of each mode. The total number of transported aerosol tracers is 31 for MAM7. The transported gas species are sulfur dioxide ( $\text{SO}_2$ ), hydrogen peroxide ( $\text{H}_2\text{O}_2$ ), dimethyl sulfide (DMS), sulfuric acid gas vapor ( $\text{H}_2\text{SO}_4$ ), ammonia ( $\text{NH}_3$ ), and a lumped semi-volatile organic species.

For long-term (decades to centuries) climate simulations, a 3-mode version of MAM (MAM3) is also developed that has only Aitken, accumulation and coarse modes (Fig. 2). For MAM3 the following assumptions are made: (1) primary carbon is internally mixed with secondary aerosol by merging the primary carbon mode with the accumulation mode; (2) the coarse dust and sea salt modes are merged into a

**Table 1.** Geometric standard deviations ( $\sigma_g$ ) and dry diameter size ranges for MAM3 and MAM7 modes. The size range values are the 10th and 90th percentiles of the global annual average number distribution for the modes (from simulations presented in Sect. 3).

Mode	$\sigma_g$	Size range ( $\mu\text{m}$ )
<b>MAM3</b>		
Aitken	1.6	0.015–0.053
Accumulation	1.8	0.058–0.27
Coarse	1.8	0.80–3.65
<b>MAM7</b>		
Aitken	1.6	0.015–0.052
Accumulation	1.8	0.056–0.26
Primary Carbon	1.6	0.039–0.13
Fine Sea Salt	2.0	0.095–0.56
Fine Dust	1.8	0.14–0.62
Coarse Sea Salt	2.0	0.63–3.70
Coarse Dust	1.8	0.59–2.75

single coarse mode based on the recognition that sources of dust and sea salt are geographically separated. Although dust is much less soluble than sea salt, it readily absorbs water (Koretsky et al., 1997) and activates similarly as CCN (Kumar et al., 2009), particularly when coated by species like sulfate and organic. So dust is likely to be removed by wet deposition almost as easily as sea salt, and the merging of dust and sea salt in a single mode is unlikely to introduce substantial error into our simulations; (3) the fine dust and sea salt modes are similarly merged with the accumulation mode; (4) sulfate is partially neutralized by ammonium in the form of  $\text{NH}_4\text{HSO}_4$ , so that ammonium is effectively prescribed and  $\text{NH}_3$  is not simulated. The total number of transported aerosol tracers in MAM3 is 15. The transported gas species are  $\text{SO}_2$ ,  $\text{H}_2\text{O}_2$ , DMS,  $\text{H}_2\text{SO}_4$ , and a lumped semi-volatile organic species. The prescribed standard deviation and the typical size range for each mode are given in Table 1.

### 3 Aerosol distributions and budgets

All simulations are performed with the stand-alone version CAM5.1, using climatological sea surface temperature and sea ice and anthropogenic aerosol and precursor gas emissions for the year 2000. The model is integrated for 6 yr, and results from the last 5 yr are used in this study. In this section model-simulated global distributions and budgets for different aerosol species are analyzed and comparisons are made between MAM3 and MAM7.

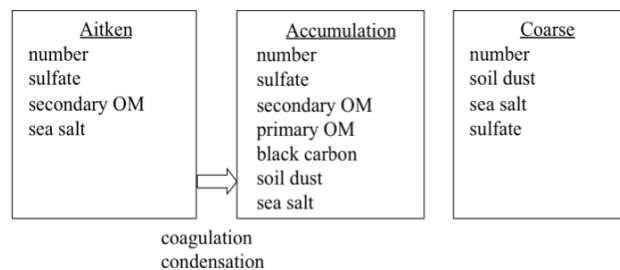


**Fig. 2.** Predicted species for interstitial and cloud-borne component of each aerosol mode in MAM3.

### 3.1 Simulated global aerosol distributions

Figures 3a and b show annual mean vertically integrated (column burden) mass concentrations of sulfate, BC, POM, SOA, dust and sea salt from MAM3, and the relative difference of these concentrations between MAM7 and MAM3, respectively. These aerosol species concentrations are summations over all available modes (e.g., the POM concentration in MAM7 includes contributions from the primary carbon and accumulation modes). Sulfate has maximum concentrations in the industrial regions (e.g., East Asia, Europe, and North America). The distribution patterns and absolute values of sulfate concentration are very similar (mostly within 10%) between MAM3 and MAM7 (Fig. 3b). This is expected since most of sulfate burden ( $\sim 90\%$ ) is in the accumulation mode (see sulfate budget in Sect. 3.2). This is also the case for SOA, which has high concentrations over the industrial regions and tropical regions with strong biogenic emissions (e.g., Central Africa and South America). The differences between MAM3 and MAM7 are generally small (mostly within 10%). POM column concentrations have spatial distributions and magnitudes similar to SOA, but are lower in Europe, Northeastern US and South America, and higher in Central Africa. The distribution patterns of BC burden concentrations are similar to those of POM, but have relatively larger contributions from the industrial regions because of different emission factors of BC/POM from different sectors. Dust burden concentrations have maxima over strong source regions (e.g., Northern Africa, Southwest and Central Asia, and Australia) and over the outflow regions (e.g., in the Atlantic and in the western Pacific). Sea salt burden concentrations are high over the storm track regions (e.g., the Southern Ocean) where wind speeds and emissions are higher, and in the subtropics of both hemispheres where precipitation scavenging is weaker.

One major difference between MAM3 and MAM7 is the treatment of primary carbonaceous aerosols (POM and BC). These aerosols are instantaneously mixed with sulfate and other components in the accumulation mode in MAM3 once they are emitted, and thus are subject to wet removal by precipitation due to the high hygroscopicity of sulfate. In MAM7, carbonaceous aerosols are emitted in the primary

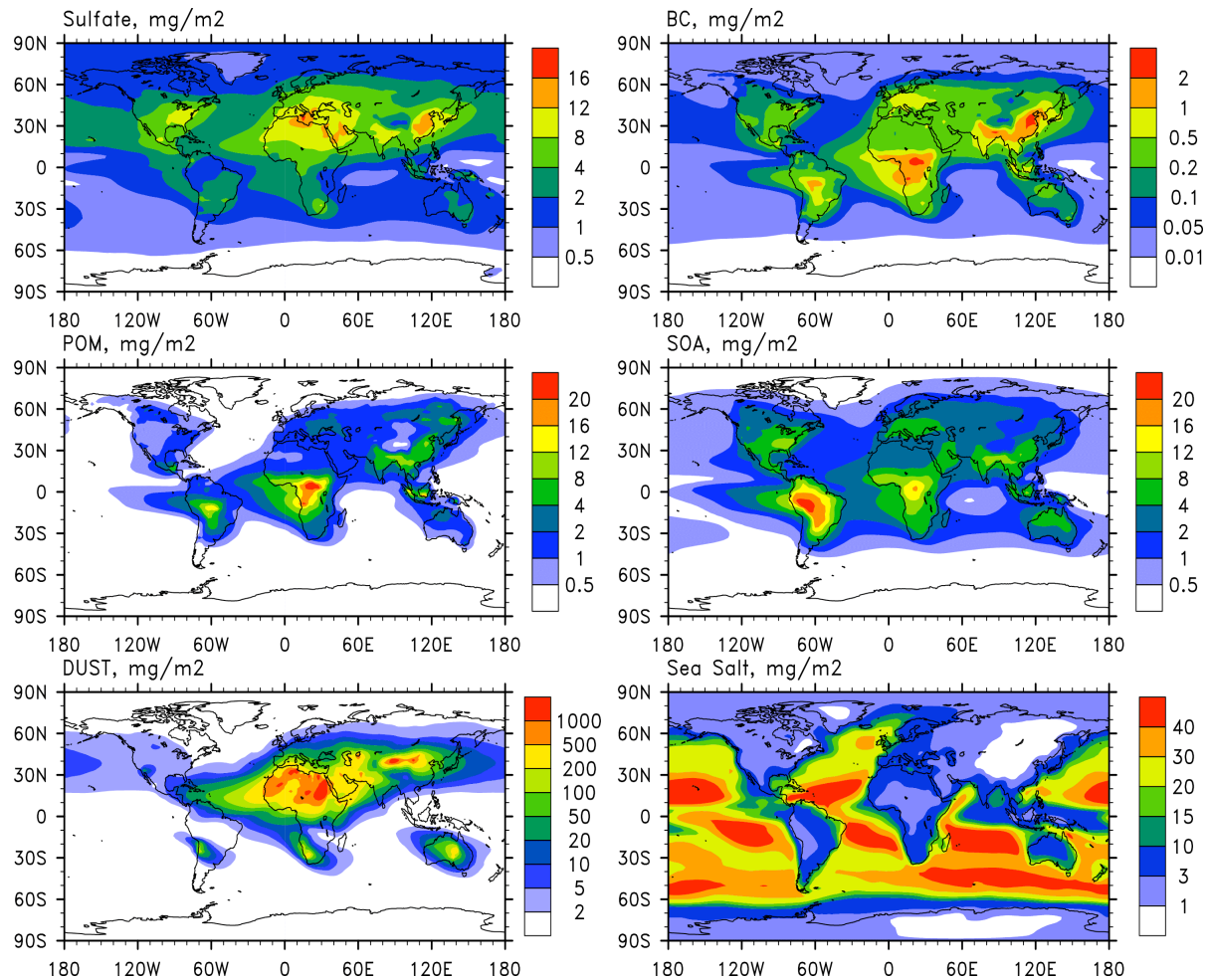


**Fig. 3a.** Annual mean vertically integrated concentrations ( $\text{mg m}^{-2}$ ) of sulfate, BC, POM, SOA, dust, and sea salt from MAM3.

carbon mode and aged to the accumulation mode by condensation of  $\text{H}_2\text{SO}_4$  vapor,  $\text{NH}_3$  and the semi-volatile organics and by coagulation with Aitken and accumulation mode. The accumulation mode has a higher volume mean hygroscopicity than that of the primary carbon mode and is subject to stronger wet removal by precipitation. Therefore, we expect higher concentrations for POM and BC in MAM7 than in MAM3. However, since we use a hygroscopicity ( $\kappa$ ) of 0.10 for POM (to account for the soluble nature of biomass burning aerosols), POM and BC in the primary carbon mode in MAM7 are subject to wet scavenging before aging into the accumulation mode. As shown in Fig. 3b, differences in column burden concentrations of POM and BC are within 10% on the global scale between MAM3 and MAM7. However, concentrations from MAM7 can be higher by up to 40% in some source regions, e.g., in Siberia and Indonesia, where  $\text{H}_2\text{SO}_4$  concentrations are lower, and thus the aging of POM and BC in the primary carbon mode is slower. The sensitivities of model results to a different hygroscopicity of POM

( $\kappa = 0.0$ ) and to a different criterion (8 monolayers) for the aging of primary carbon mode aerosols will be described in Sect. 5.

Other major differences between MAM3 and MAM7 are cut-off size ranges of emissions and the mixing states assumed for dust and sea salt, as discussed in Sect. S1.1 of the Supplement. The fine dust mode is separated from the accumulation mode in MAM7, while in MAM3 it is merged into the accumulation mode. There is a fine sea salt mode in MAM7, which is merged into the accumulation mode in MAM3. Coarse dust and sea salt mode in MAM7 are merged into a single coarse mode in MAM3. Dust column burden concentrations are generally higher in MAM7 (Fig. 3b) with global dust burden increased by  $\sim 10\%$ . In some regions away from dust sources, the difference can reach 60%. This will be further discussed in the budget analysis in Sect. 3.2. Significant changes occur for sea salt with sea salt column burden concentrations reduced by  $\sim 30\%$  in MAM7. Besides differences in mixing states and cut-off size ranges of

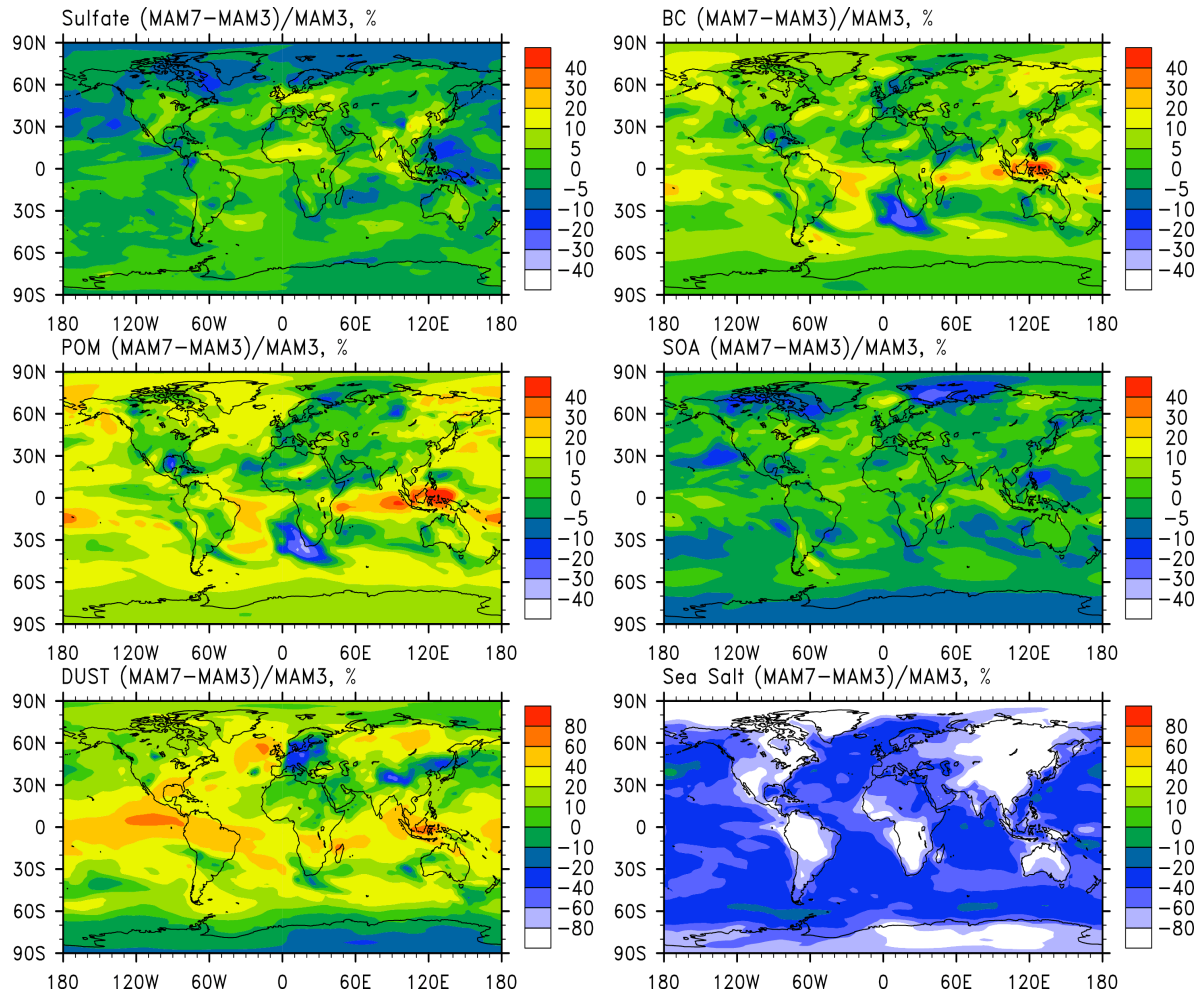


**Fig. 3b.** Relative differences (in %) of annual mean vertically integrated concentrations of sulfate, BC, POM, SOA, dust, and sea salt between MAM7 and MAM3.

sea salt, the standard deviations  $\sigma_g$  of log-normal distributions are reduced from 2.0 for fine and coarse sea salt modes in MAM7 to 1.8 for the accumulation and coarse mode in MAM3 for the merging with other species. The larger  $\sigma_g$  in MAM7 increases the mass-weighted sedimentation velocity of coarse-mode sea salt by about 65 %, which causes the lower sea salt mass concentrations in MAM7.

Figure 4 shows the annual and zonal mean distributions of sulfate, BC, POM, SOA, dust and sea salt mass concentrations in MAM3. Anthropogenic sulfate in the Northern Hemisphere (NH) mid-latitudes is lifted upward and transported towards the North Pole in the upper troposphere. Other peak concentrations of BC, POM and SOA near the tropics in the biomass burning regions are transported upwards and towards the upper troposphere in the Southern Hemisphere (SH). Dust particles are uplifted into the free troposphere, since dust emission is often produced by frontal systems (Merrill et al., 1989). In comparison, sea salt is

mostly confined below 700 hPa. This is because sea salt particles have larger wet sizes due to the water uptake over the oceans, which produces stronger wet removal and gravitational settling of sea salt particles towards the surface. Consistent with Fig. 3b, sea salt concentration in the zonal mean distribution is lower in MAM7 than that in MAM3 mainly due to the larger standard deviations of log-normal distributions for fine and coarse sea salt modes in MAM7, while differences are much smaller for other aerosol species (figures not shown). Concentrations of BC, POM, SOA, and dust are all very low in the lower troposphere at NH high latitudes, due to efficient wet removal during transport from source regions.

Figure 5 shows the annual mean number concentration of aerosol in Aitken, accumulation and coarse mode in the surface layer from MAM3 and MAM7 at standard temperature and pressure (1013.25 hPa, 273.15 K). For a direct comparison with MAM3, we show an “equivalent” accumulation

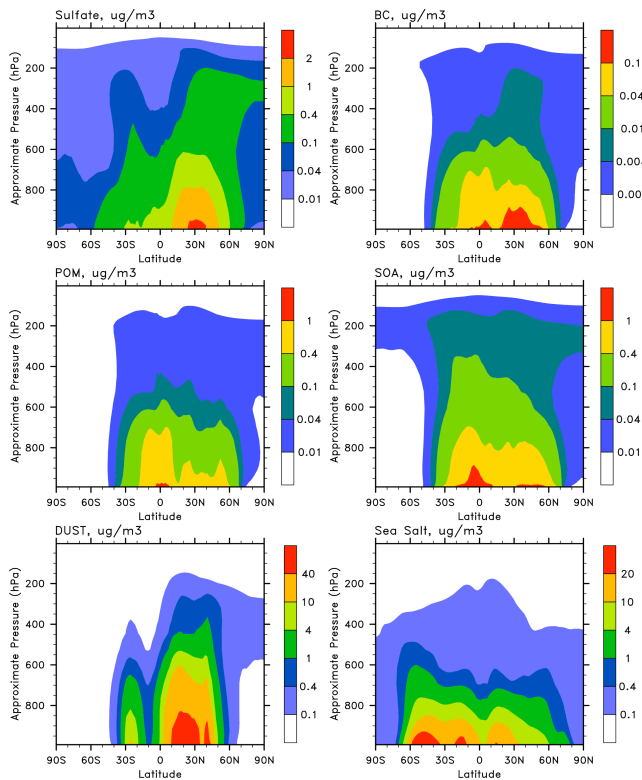


**Fig. 4.** Annual and zonal mean distributions of sulfate, BC, POM, SOA, dust and sea salt concentrations in MAM3.

mode number concentration for MAM7, which is the sum of the aerosol number concentrations in the MAM7 accumulation, primary carbon, and fine sea salt modes, and the sub-micron (diameter  $< 1.0 \mu\text{m}$ ) portion of the fine dust mode. In the same way, the equivalent coarse mode number concentration is the sum of the aerosol number concentrations in the MAM7 coarse sea-salt and dust modes and the super-micron portion of the fine dust mode. As indicated in Fig. 5, accumulation mode number concentrations in both MAM3 and MAM7 are higher over the continents due to the primary emissions of sulfate, POM and BC, and growth of aerosol particles from Aitken to accumulation mode. In the industrial regions (e.g., East and South Asia and Europe) and in the biomass burning regions (e.g., maritime continent, Central Africa, South America, Siberia), the number concentration can exceed  $1000 \text{ cm}^{-3}$ . Accumulation mode number concentrations over oceans can be high in the continental outflow regions (e.g., west Pacific, tropical Atlantic), while in the remote areas, the concentrations are less than  $100 \text{ cm}^{-3}$ . We do not find significant differences in accumulation mode aerosol number concentrations between MAM3 and MAM7. A breakdown of contributions from individual modes to the MAM7 equivalent (total) accumulation mode number concentration (shown in Fig. 5) is as follows: the fine sea-salt mode contributes about  $5\text{--}20 \text{ cm}^{-3}$  over oceans; the fine dust

mode contributes  $50\text{--}100 \text{ cm}^{-3}$  over major source regions (e.g., Northern Africa and North China) and  $10\text{--}20 \text{ cm}^{-3}$  in the dust outflow regions; the primary carbon mode contributes  $200\text{--}2000 \text{ cm}^{-3}$  over the industrial region (e.g., East Asia and Europe) and  $500\text{--}3000 \text{ cm}^{-3}$  in the biomass burning regions (e.g., Central Africa, South America, Indonesia, and Russia), and the rest is from the accumulation mode.

Aerosol number concentrations in the Aitken mode in MAM3 and MAM7 are high over the continents with strong sulfur emissions (e.g., in East Asia, Europe, and in North America). Aitken mode aerosol number concentrations are very low (less than  $40 \text{ cm}^{-3}$ ) in the biomass burning regions, because primary aerosol particles from the biomass burning source are emitted in the accumulation mode in MAM3 and in the primary carbon mode in MAM7, in both cases with a  $0.08 \mu\text{m}$  number mode diameter (see Table S1 in the Supplement). Over remote oceanic regions, aerosol number concentrations in Aitken mode can reach  $500 \text{ cm}^{-3}$ . This is primarily due to strong aerosol nucleation in these regions where there are extremely few ( $< 40 \text{ cm}^{-3}$ ) accumulation mode aerosol particles available for condensation to compete with the nucleation, but there are modest sources of  $\text{SO}_2$  (from DMS oxidation) and thus  $\text{H}_2\text{SO}_4$ . These make conditions favorable for nucleation. Sea salt emissions also contribute to the Aitken mode number in the SH storm track region near  $60^\circ \text{S}$  where surface winds are strong. We see higher Aitken mode number concentrations in MAM7 than those in MAM3 over these remote regions.  $\text{H}_2\text{SO}_4$  concentrations are somewhat higher in MAM7, due to the lower sea salt mass concentration in MAM7 and thus slower  $\text{H}_2\text{SO}_4$  condensational loss in the marine boundary layer compared to MAM3. This results in more aerosol nucleation in MAM7. Aerosol number concentrations in the coarse mode are higher over the sea salt and dust source regions and in the dust outflow regions and are in the range of  $2\text{--}10 \text{ cm}^{-3}$ . Interestingly, even though sea salt mass concentrations in the coarse mode in MAM3 are significantly higher than in MAM7 over the oceanic regions, coarse mode aerosol number concentrations are similar between MAM3 and MAM7. This is because the number-weighted settling velocity for coarse mode sea salt number is rather insensitive to small  $\sigma_g$  changes. As a result, the coarse mode median diameters are larger in MAM3 due to higher mass concentrations (figure not shown).

Figure 6 is the same as Fig. 5 except for annual and zonal mean aerosol number concentrations in Aitken, accumulation and coarse modes. Aitken mode aerosol number concentrations show a prominent peak caused by nucleation in the tropical upper troposphere and over the South Pole, where temperature is low and relative humidity (RH) is high along with low pre-existing aerosol surface areas. Note that MAM accounts for the number loss of the new particles by coagulation as they grow from the critical cluster size (a few nanometers) to Aitken mode size ( $0.015\text{--}0.06 \mu\text{m}$ ). Consistent with surface number concentrations shown in Fig. 5, Aitken mode aerosol number concentrations

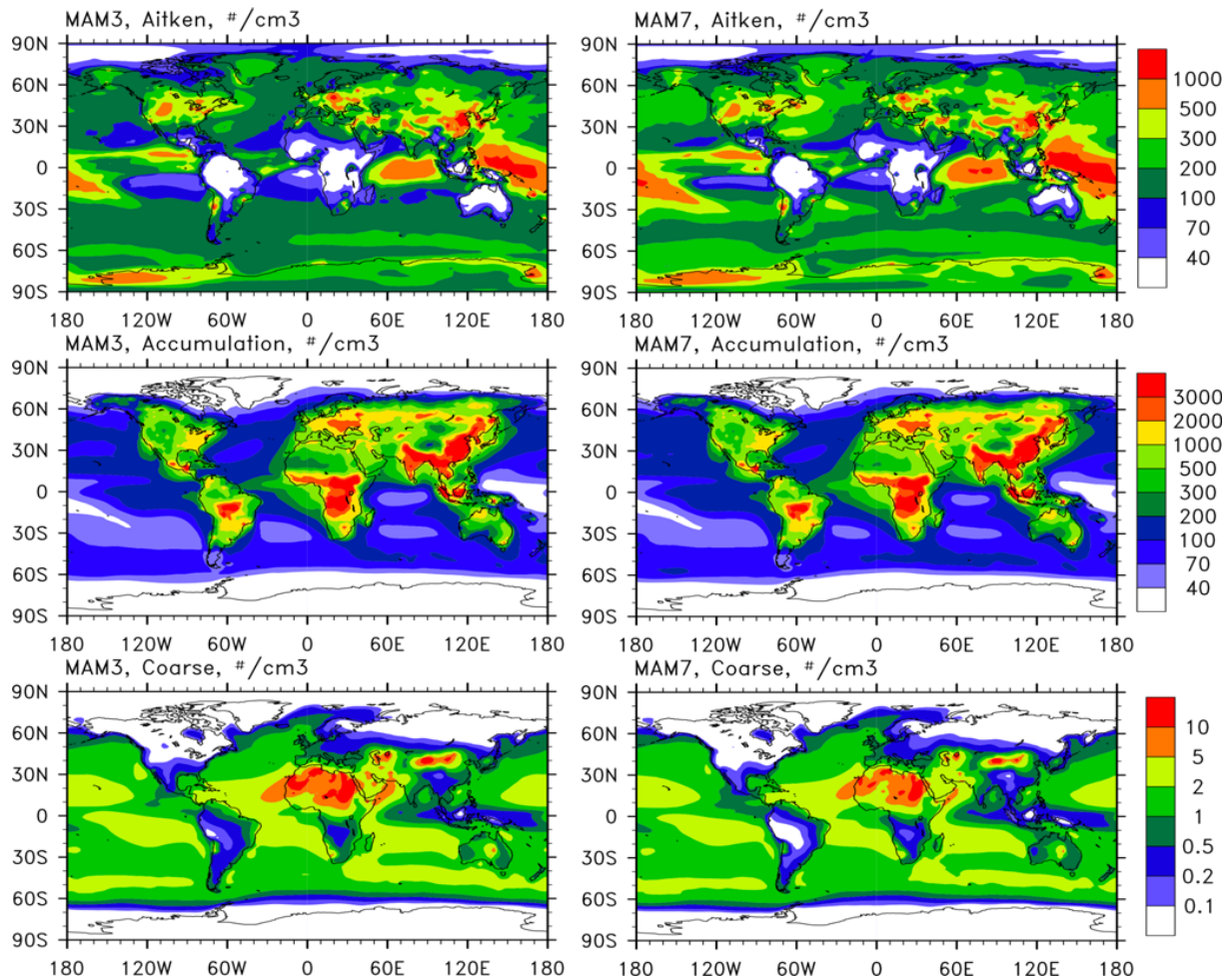


**Fig. 5.** Annual mean number concentration of aerosol in Aitken, accumulation and coarse mode in the surface layer from MAM3 (left) and MAM7 (right) at standard temperature and pressure (1013.25 hPa, 273.15 K).

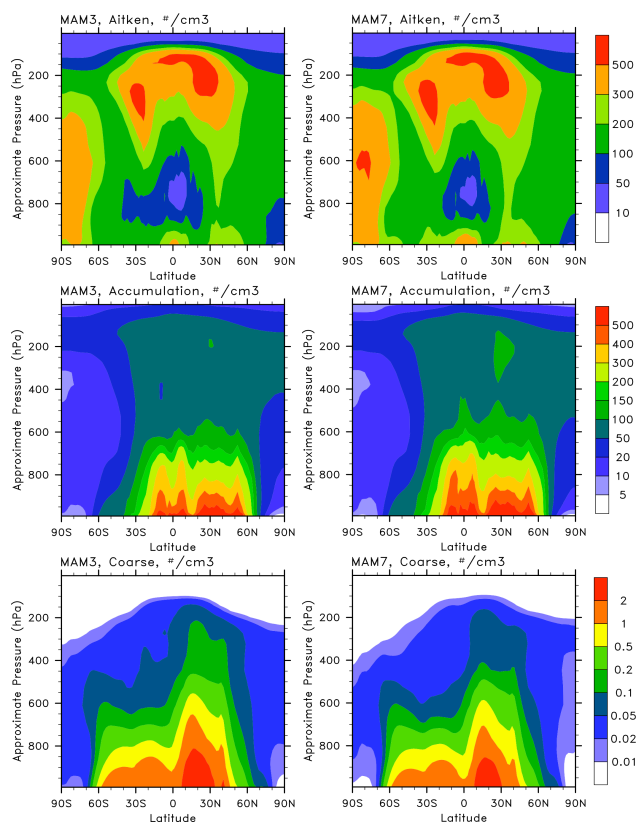
are generally higher in MAM7 than in MAM3. Accumulation mode aerosol particles are transported into the middle and upper troposphere with number concentrations of 20–100  $\text{cm}^{-3}$  above 600 hPa. This is contributed from biomass burning emission injected at 0–6 km in the tropics. The spatial distribution of coarse mode aerosol number concentration is associated with the spatial distribution of dust and sea salt (Fig. 4), and slightly higher number concentrations are simulated with MAM3 than with MAM7.

Figure 7 shows the annual averaged global distribution of CCN number concentration at 0.1% supersaturation ( $\text{CCN}_{0.1}$ ) in the surface layer in MAM3 and MAM7. Distribution patterns of  $\text{CCN}_{0.1}$  concentration closely follow those of accumulation mode number concentration and have high concentrations (400–1000  $\text{cm}^{-3}$ ) in the industrial regions due to the dominance of sulfate with its high hygroscopicity.  $\text{CCN}_{0.1}$  concentration has similar ranges in the biomass burning regions as in the industrial regions, because POM is assumed to be moderately hygroscopic ( $\kappa = 0.1$ ).

$\text{CCN}_{0.1}$  concentration is lower than 100  $\text{cm}^{-3}$  over oceans, except in the continental outflow regions.  $\text{CCN}_{0.1}$  concentration is 20–40% of the total accumulation mode number over the continents and outflow regions. Over the remote oceans,  $\text{CCN}_{0.1}$  concentration is 70–90% of accumulation mode aerosol number concentration.  $\text{CCN}_{0.1}$  concentration in MAM3 is higher than that in MAM7 over the oceanic regions. This is due to merging of the 0.3–1.0  $\mu\text{m}$  size range of MAM7 fine sea salt into the accumulation mode in MAM3, increasing MAM3 accumulation mode median size, and thus allowing more of the accumulation mode particles to be CCN at 0.1% supersaturation, although coarse mode aerosol number concentrations are similar there (Fig. 5).

### 3.2 Annual global budgets of aerosols and precursor gases

Tables 2–8 give the global budgets of aerosol species and their precursor gases in MAM3 and MAM7. Budgets of gas species are compared to a range of model results collected



**Fig. 6.** Same as Fig. 5, except for annual and zonal mean aerosol number concentrations in Aitken, accumulation and coarse mode.

from literature by Liu et al. (2005). For aerosol species, the averages and standard deviations of available models that participated in the AeroCom project (Textor et al., 2006) are listed for comparison as “AeroCom”.

The DMS emission from ocean is  $18.2 \text{ Tg S yr}^{-1}$ , which is balanced by the gas-phase oxidation of DMS to form  $\text{SO}_2$  and other products (e.g., MSA). DMS burden is  $0.067 \text{ Tg S}$  with a lifetime of 1.3 days for both MAM3 and MAM7 (Table 2), which is within the range of model results reported in the literature.  $\text{SO}_2$  emission ( $64.8 \text{ Tg S yr}^{-1}$ ) is at the low end of the range of model results. Production of  $\text{SO}_2$  from DMS oxidation ( $15.2 \text{ Tg S yr}^{-1}$ ) together with  $\text{SO}_2$  emission is balanced by  $\text{SO}_2$  losses by dry and wet deposition, and by gas- and aqueous-phase oxidation. The wet deposition loss of  $\text{SO}_2$  is at the high end of the range from the literature and is comparable to that of dry deposition loss. This is because wet deposition of gas species in CAM5 uses the MOZART treatment (Emmons et al., 2010), which assumes that the wet removal rate coefficient of  $\text{SO}_2$  is the same as that of  $\text{H}_2\text{O}_2$  and assumes full gas retention during droplet freezing. 66–68 % of chemical loss of  $\text{SO}_2$  is through the aqueous-phase oxidation. One noticeable difference between MAM3 and MAM7 is the larger aqueous-phase oxidation in MAM7. This is because  $\text{NH}_3$  and ammonium are explicitly treated in MAM7,

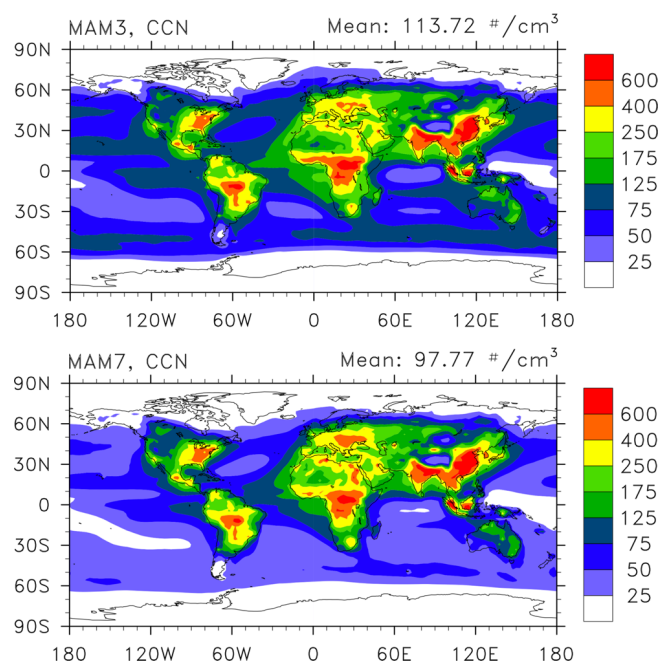


**Fig. 7.** Annual averaged global distribution of CCN number concentration at 0.1 % supersaturation at surface in MAM3 (upper) and MAM7 (lower).

and  $\text{NH}_3$  dissolves in cloud water to increase pH values to be larger than those with the assumed form of  $\text{NH}_4\text{HSO}_4$  in MAM3 (figure not shown). Thus, this enhances the aqueous-phase  $\text{SO}_2$  oxidation by  $\text{O}_3$  (Seinfeld and Pandis, 1998). The global burden of  $\text{SO}_2$  is  $0.35 \text{ (MAM3)}$  and  $0.34 \text{ Tg S (MAM7)}$  with a lifetime of 1.60 (MAM3) and 1.55 days (MAM7), which are within the range of the literature.

$\text{H}_2\text{SO}_4$  vapor is produced by gas-phase  $\text{SO}_2$  oxidation and is lost primarily by condensation onto pre-existing aerosol (96 %) and also by aqueous-phase uptake by cloud water (4 %) (Table 2). The losses by dry deposition (0.01 %) and nucleation (0.2 %) are negligibly small.  $\text{H}_2\text{SO}_4$  vapor has a global burden of  $\sim 0.00040 \text{ Tg S}$ , and a lifetime of 15 min, longer than limited reports from the literature.

Sulfate aerosol is produced from aqueous-phase  $\text{SO}_2$  oxidation and to a lesser extent from  $\text{H}_2\text{SO}_4$  condensation on pre-existing aerosol, and is lost mainly by wet scavenging (Table 3). MAM7 has a smaller percentage of aqueous-phase sulfate production from  $\text{H}_2\text{O}_2$  compared to MAM3 for the reason mentioned above. The global burden is  $\sim 0.46 \text{ Tg S}$ , which is lower than the AeroCom multi-model mean. The lifetime is 3.7–3.8 days, which is close to the AeroCom multi-model mean (4.12 days). The lower sulfate burden is primarily due to its smaller sources ( $44\text{--}46 \text{ Tg S yr}^{-1}$ ) compared to AeroCom multi-model mean ( $59.67 \text{ Tg S yr}^{-1}$ ). Most sulfate (89–96 %) is in the accumulation mode, which has a larger total surface area for  $\text{H}_2\text{SO}_4$  condensation and a higher contribution of cloud droplet number concentration for aqueous-phase oxidation.

**Table 2.** Global budgets for DMS, SO<sub>2</sub>, and H<sub>2</sub>SO<sub>4</sub> in MAM3 and MAM7. The range of results from other studies is from Liu et al. (2005) and references therein.

	MAM3	MAM7	Previous studies Liu et al. (2005)
DMS			
Sources	18.2	18.2	
Emission	18.2	18.2	10.7–23.7
Sinks	18.2	18.3	
Gas-phase oxidation	18.2	18.3	10.7–23.7
Burden	0.067	0.067	0.02–0.15
Lifetime	1.34	1.32	0.5–3.0
SO <sub>2</sub>			
Sources	80.0	80.0	
Emission	64.8	64.8	63.7–92.0
DMS oxidation	15.2	15.2	10.0–24.7
Sinks	79.9	79.8	
Dry deposition	19.7	19.0	16.0–55.0
Wet deposition	17.6	16.8	0.0–19.9
Gas-phase oxidation	14.5	14.3	6.1–16.8
Aqueous-phase oxidation	28.0	29.7	24.5–57.8
Burden	0.35	0.34	0.20–0.61
Lifetime	1.60	1.55	0.6–2.6
H <sub>2</sub> SO <sub>4</sub>			
Sources	14.5	14.3	
Gas-phase production	14.5	14.3	6.1–22.0
Sinks	14.5	14.3	
Dry deposition	0.002	0.003	
Aqueous-phase uptake	0.59	0.51	
Nucleation	0.030	0.030	
Condensation	13.9	13.7	
Burden	0.00040	0.00042	$9.0 \times 10^{-6}$ – $1.0 \times 10^{-3}$
Lifetime (min)	14.5	15.3	7.3–10.1

Units are sources and sinks, Tg S yr<sup>-1</sup>; burden, Tg S; lifetime, days except for H<sub>2</sub>SO<sub>4</sub> (min).

The NH<sub>3</sub> and NH<sub>4</sub> cycles are explicitly treated in MAM7. Their budgets are given in Table 4. The source of NH<sub>3</sub> from emission is balanced by losses due to the condensation onto pre-existing aerosol to form NH<sub>4</sub> and to a lesser extent due to dry and wet deposition. The global NH<sub>3</sub> burden is 0.064 Tg N with a lifetime of 0.48 days. The formation of NH<sub>4</sub> from condensation is balanced by the loss, mostly due to wet deposition. The global NH<sub>4</sub> burden is 0.24 Tg N with a lifetime of 3.4 days. There is a small budget term for NH<sub>3</sub> and NH<sub>4</sub> related to the partitioning between NH<sub>3</sub> and NH<sub>4</sub> in cloud water, based on the effective Henry's law. NH<sub>3</sub> and NH<sub>4</sub> budgets are compared to a few available studies in the literature (Table 4). The NH<sub>3</sub> and NH<sub>4</sub> budgets are close to those from a modeling study by Feng and Penner (2007), although our burdens are slightly lower and lifetimes slightly shorter. The molar ratio of ammonium to sulfate (NH<sub>4</sub>/SO<sub>4</sub>) in aerosol has a global annual average value of 1.2. In the continental boundary layer, it is near 2 for many regions but is lower over

desert, boreal, and polar regions, with lowest values (annual average < 0.1) over Antarctica. In the marine boundary layer, the ratio is near 2 in the tropics, is generally less than 1.0 in the NH mid-latitudes, and is in the 0.5–1.5 range in the SH mid-latitudes. The ratio is less than 1.0 in much of the free troposphere, except in the tropics where ratios of 1.5–2.0 appear, especially over continents. These results indicate different neutralization of SO<sub>4</sub> by NH<sub>4</sub> in aerosol in MAM7, compared to a molar ratio of 1.0 with NH<sub>4</sub>H<sub>2</sub>SO<sub>4</sub> assumed in MAM3.

Table 5 gives the budgets of POM and SOA. The POM burden is 0.63–0.68 Tg, which is less than half of the AeroCom mean (1.7 Tg). This is mainly because the Intergovernmental Panel on Climate Change (IPCC) Fifth Assessment Report (AR5) POM emissions used here (Sect. S1.1.1 in the Supplement) are only about half of the AeroCom multi-model mean. Also, for many of the AeroCom models, biogenic SOA is included in the POM. The POM lifetime is 4.5–4.9 days,

**Table 3.** Global annual budget for sulfate. The means and normalized standard deviations (in %) from available models participating in AeroCom (Textor et al., 2006) are listed. The values in parentheses are mean removal rates (in  $\text{day}^{-1}$ ), and normalized standard deviations (in %) as budget terms are not given in Textor et al. (2006). For comparison, removal rates (in  $\text{day}^{-1}$ ) from MAM3 and MAM7 are listed in parentheses.

	MAM3	MAM7	AeroCom
Sources	44.30	45.71	59.67, 22
Emission	1.66	1.66	
SO <sub>2</sub> aqueous-phase oxidation	28.03	29.74	
from H <sub>2</sub> O <sub>2</sub> chemistry (%)	53.9	48.1	
H <sub>2</sub> SO <sub>4</sub> aqueous-phase uptake	0.59	0.51	
H <sub>2</sub> SO <sub>4</sub> nucleation	0.030	0.030	
H <sub>2</sub> SO <sub>4</sub> condensation	13.98	13.74	
Sinks	44.30	45.71	
Dry deposition	4.96 (0.03)	5.51 (0.03)	(0.03, 55)
Wet deposition	39.34 (0.23)	40.20 (0.23)	(0.22, 22)
Burden	0.46	0.47	0.66, 25
In modes (%)	2.8 (Aitken), 95.5 (accum.), 1.7 (coarse)	2.9 (Aitken), 88.9 (accum.), 1.1 (fine sea salt), 5.9 (fine dust), 0.32 (coarse sea salt), 0.88 (coarse dust)	
Lifetime	3.77	3.72	4.12, 18

Units are sources and sinks, Tg S yr<sup>-1</sup>; burden, Tg S; lifetime, days.

which is lower than that of the AeroCom multi-model mean (6.54 days), due to the higher wet removal rates in this study (0.19 d<sup>-1</sup> in MAM3 and 0.17 d<sup>-1</sup> in MAM7 in Table 5) compared to the AeroCom mean (0.14 d<sup>-1</sup> in Table 5). We note that the wet removal rate for sulfate in this study (0.23 d<sup>-1</sup>) is close to that (0.22 d<sup>-1</sup>) of the AeroCom multi-model mean, and thus the sulfate lifetimes are similar between this study and the AeroCom multi-model mean (Table 3). This reflects the fact that a lower scavenging efficiency was often used for POM than for sulfate in AeroCom models (Textor et al., 2006), while in MAM the wet removal rates for POM and sulfate are similar due to the rapid (MAM7) or instantaneous (MAM3) aging of POM. The POM burden is slightly lower and lifetime slightly shorter in MAM3 than in MAM7 due to the instant aging of POM and mixing with sulfate and other components in the accumulation mode in MAM3, which produces faster wet removal due to the higher hygroscopicity of sulfate than that of POM (Table S3 in the Supplement). In MAM7, about 15 % of POM is in the primary carbon mode and has a lifetime of 0.72 days due to the fast aging to the accumulation mode. The burden of SOA is 1.15 Tg and has a lifetime of 4.1 days. The SOA lifetime is shorter than that of POM. This is confirmed by the larger wet removal rate (by 20–30 %) of SOA than that of POM. The reason is that SOA is formed from the partitioning of semi-volatile organic gas species emitted at the surface in the model and thus experiences wet removal by precipitation in the boundary layer, while biomass burning emissions are elevated and occur in

different seasons and different geographical regions. Another reason for the shorter SOA lifetime is the larger hygroscopicity (0.14) of SOA than that (0.10) of POM. The SOA burden is higher and lifetime shorter than the means from other studies collected in Farina et al. (2010), which, however, have very large standard deviations (> 100 %).

The simulated global BC burden is 0.088–0.093 Tg (Table 6), which is only 40 % of AeroCom multi-model mean (0.24 Tg). One reason for the difference is that the IPCC AR5 BC emission is 65 % of the AeroCom multi-model mean. Another reason is that the wet removal rate is 60 % higher in this model than the AeroCom multi-model mean. The higher wet removal rate in this study can be due to the rapid (MAM7) or instantaneous (MAM3) aging of BC in this study (thus a similar wet removal rate of 0.19–0.20 d<sup>-1</sup> for BC in Table 6 compared to 0.23 d<sup>-1</sup> for sulfate in Table 3). In comparison, the wet removal rate of BC (0.12 d<sup>-1</sup>) of the AeroCom multi-model mean is much lower than that of sulfate (0.22 d<sup>-1</sup>) due to a lower scavenging efficiency often used for BC than for sulfate in AeroCom models (Textor et al., 2006). The simulated BC lifetime is 4.2–4.4 days, much lower than the AeroCom multi-model mean (7.1 days). BC burden is slightly higher and lifetime slightly longer in MAM7 than in MAM3. About 10 % of BC is in the primary carbon mode with a lifetime of 0.47 days in MAM7, which is shorter than that of POM (0.73 days). BC has relatively more fossil fuel and less biomass burning emissions compared to POM. As there are higher SO<sub>2</sub> emissions and more H<sub>2</sub>SO<sub>4</sub> for condensation in

**Table 4.** Global budgets for NH<sub>3</sub> gas and NH<sub>4</sub> aerosol in MAM7. The range of results from other studies is from Feng and Penner (2007) and references therein.

	MAM7	Previous studies Feng and Penner (2007)
NH <sub>3</sub>		
Sources	48.8	
Emission	46.0	52.1–54.1
Gas/aqueous-phase partitioning	2.8	
Sinks	48.9	
Dry deposition	12.5	15.4–29.4
Wet deposition	10.4	7.4–16.7
Nucleation	0.014	
Condensation	26.0	
Burden	0.064	0.084–0.19
Lifetime	0.48	0.57–1.4
NH <sub>4</sub>		
Sources	26.0	4.5–26.1
NH <sub>3</sub> condensation	26.0	
NH <sub>3</sub> nucleation	0.014	
Sinks	26.1	
Dry deposition	3.4	0.2–6.6
Wet deposition	19.9	4.3–23.0
Gas/aqueous-phase partitioning	2.8	
Burden	0.24	0.045–0.30
In modes (%)	1.8 (Aitken), 89.9 (accum.), 1.5 (fine sea salt), 5.7 (fine dust), 0.42 (coarse sea salt), 0.74 (coarse dust)	
Lifetime	3.4	3.6–4.2

Units are sources and sinks, Tg N yr<sup>-1</sup>; burden, Tg N; lifetime, days.

the industrial regions than in the biomass burning regions, overall BC ages faster than POM.

Table 7 gives the budgets for dust. The simulated dust emission (2900–3100 Tg yr<sup>-1</sup>) is ~60 % higher than the AeroCom multi-model mean (1840 Tg yr<sup>-1</sup>), and dust has a burden of 22–25 Tg, close to the AeroCom multi-model mean (19 Tg) because of the shorter lifetime (2.6–3.1 days) in the simulation than the AeroCom mean (4.14 days). The reason for the shorter lifetime is due to the larger wet removal rate (by ~60 %) than the AeroCom mean. Gravitational settling plays a dominant role (~90 %) in the total dry deposition, larger than the AeroCom mean (46.2 %). The burden is slightly lower and lifetime shorter in MAM3 than in MAM7, respectively. This is due to the larger dry deposition rate in MAM3, with a different emission cut-off size from that in MAM7. The internal mixing of dust with other components in MAM3 also increases the wet removal rate of dust in MAM3 compared to that in MAM7. The sensitivity of simulated dust to different emission cut-off sizes will be investigated in a future study.

The simulated sea salt emission is ~5000 Tg yr<sup>-1</sup>, slightly lower than the AeroCom median (6280 Tg yr<sup>-1</sup>), and substantially lower than the AeroCom mean (16 600 Tg yr<sup>-1</sup>) with a standard deviation of ~200 % (Table 8). Note that some of the AeroCom models treated sea salt larger than 10 μm diameter. The burden is 7.58 Tg and lifetime 0.55 day in MAM7, similar to the AeroCom means. The dry and wet deposition rates are close to the AeroCom medians, and so is the contribution of sedimentation to dry deposition (60.8 %) in MAM7. In MAM3, the wet deposition rate does not change much from that in MAM7. However, the dry deposition rate is ~40 % less, due to the smaller standard deviation  $\sigma_g$  of the coarse mode in MAM3 (1.8), compared with that for coarse sea salt mode in MAM7 (2.0). Therefore, the sea salt burden in MAM3 is 10.4 Tg and lifetime 0.76 day, which is ~37 % higher than that in MAM7, respectively. Most (~90 %) of sea salt is in the coarse mode in both MAM3 and MAM7.

**Table 5.** Global budgets for POM and SOA. For POM, the means and normalized standard deviations (in %) from available models participating in AeroCom (Textor et al., 2006) are listed. The values in parentheses are mean removal rates (in  $\text{day}^{-1}$ ), and normalized standard deviations (in %) as budget terms are not given in Textor et al. (2006). For comparison, removal rates (in  $\text{day}^{-1}$ ) from MAM3 and MAM7 are listed in parentheses. For SOA, the mean and normalized standard deviations (in %) from other studies are from Farina et al. (2010) and references therein.

	MAM3	MAM7	AeroCom/Other studies
POM			
Sources	50.2	50.2	96.6, 26
Fossil and bio-fuel emission	16.8	16.8	
Biomass burning emission	33.4	33.4	
Sinks	50.1	50.1	
Dry deposition	7.4 (0.03)	8.4 (0.03)	(0.03, 49)
Wet deposition	42.7 (0.19)	41.7 (0.17)	(0.14, 32)
Burden	0.63	0.68	1.70, 27
In modes (%)	100 (accum.)	14.7 (primary carbon) 85.3 (accum.)	
Lifetime	4.56	4.90	6.54, 27
SOA			
Sources	103.3	103.3	34.0, 123
Condensation of SOA (g)	103.3	103.3	
Sinks	103.2	103.2	
Dry deposition	11.2 (0.03)	11.3 (0.03)	
Wet deposition	92.0 (0.22)	91.9 (0.22)	
Burden	1.15	1.15	0.57, 117
In modes (%)	0.8 (Aitken) 99.2 (accum.)	1.0 (Aitken) 99.0 (accum.)	
Lifetime	4.08	4.08	6.70, 115

Units are sources and sinks,  $\text{Tg yr}^{-1}$ ; burden,  $\text{Tg}$ ; lifetime, days.

**Table 6.** Global budgets for BC. The means and normalized standard deviations (in %) from available models participating in AeroCom (Textor et al., 2006) are listed. The values in parentheses are mean removal rates (in  $\text{day}^{-1}$ ), and normalized standard deviations (in %) as budget terms are not given in Textor et al. (2006). For comparison, removal rates (in  $\text{day}^{-1}$ ) from MAM3 and MAM7 are listed in parentheses.

	MAM3	MAM7	AeroCom
Sources	7.76	7.76	11.9, 23
Fossil and bio-fuel emission	5.00	5.00	
Biomass burning emission	2.76	2.76	
Sinks	7.75	7.75	
Dry deposition	1.27 (0.04)	1.41 (0.04)	(0.03, 55)
Wet deposition	6.48 (0.20)	6.34 (0.19)	(0.12, 31)
Burden	0.088	0.093	0.24, 42
In modes (%)	100 (accum.)	10.8 (primary carbon) 89.2 (accum.)	
Lifetime	4.17	4.37	7.12, 33

Units are sources and sinks,  $\text{Tg yr}^{-1}$ ; burden,  $\text{Tg}$ ; lifetime, days.

## 4 Model evaluation

### 4.1 Aerosol mass concentration

Figures 8 and 9 compare simulated annual mean  $\text{SO}_2$  and sulfate concentrations at the surface from MAM3 and MAM7 with observations from the Interagency Monitoring of Protected Visual Environment (IMPROVE) sites in the United

States (<http://vista.cira.colostate.edu/improve>) and the European Monitoring and Evaluation Programme (EMEP) sites (<http://www.emep.int>). Clearly, the model overestimates  $\text{SO}_2$  in both Eastern and Western United States, while it performs better at the European EMEP sites, although there are still overestimations there. Overall, modeled sulfate agrees with observations within a factor of 2 for most sites in the United States and Europe. Sulfate in the Western United

**Table 7.** Global budgets for dust. The means, medians and normalized standard deviations (in %) from available models participating in AeroCom (Textor et al., 2006) are listed. The values in parentheses are mean and median removal rates (in  $\text{day}^{-1}$ ), and normalized standard deviations (in %) as budget terms are not given in Textor et al. (2006). For comparison, removal rates (in  $\text{day}^{-1}$ ) from MAM3 and MAM7 are listed in parentheses.

	MAM3	MAM7	AeroCom
Sources	3121.9	2943.5	1840.0, 1640.0, 49
Sinks	3122.4	2945.6	
Dry deposition	1948.4 (0.24)	1732.7 (0.19)	(0.23, 0.16, 84)
from gravitational settling (%)	89.7	89.1	46.2, 40.9, 66
Wet deposition	1174.0 (0.14)	1212.9 (0.13)	(0.08, 0.09, 42)
Burden	22.4	24.7	19.2, 20.5, 40
In modes (%)	8.0 (accum.) 92.0 (coarse)	29.5 (fine) 70.5 (coarse)	
Lifetime	2.61	3.07	4.14, 4.04, 43

Units are sources and sinks,  $\text{Tg yr}^{-1}$ ; burden,  $\text{Tg}$ ; lifetime, days.

**Table 8.** Global budgets for sea salt. The means, medians and normalized standard deviations (in %) from available models participating in AeroCom (Textor et al., 2006) are listed. The values in parentheses are mean and median removal rates (in  $\text{day}^{-1}$ ), and normalized standard deviations (in %) as budget terms are not given in Textor et al. (2006). For comparison, removal rates (in  $\text{day}^{-1}$ ) from MAM3 and MAM7 are listed in parentheses.

	MAM3	MAM7	AeroCom
Sources	4965.5	5004.1	16600.0, 6280.0, 199
Sinks	4962.9	5001.3	
Dry deposition	2410.3 (0.64)	3073.8 (1.11)	(4.28, 1.40, 219)
from gravitational settling (%)	56.6	60.8	58.9, 59.5, 65
Wet deposition	2552.6 (0.67)	1927.4 (0.70)	(0.79, 0.68, 77)
Burden	10.37	7.58	7.52, 6.37, 54
In modes (%)	~0.0 (Aitken) 7.5 (accum.) 92.5 (coarse)	~0.0 (Aitken) 1.1 (accum.) 8.0 (fine sea salt) 90.9 (coarse sea salt)	
Lifetime	0.76	0.55	0.48, 0.41, 58

Units are sources and sinks,  $\text{Tg yr}^{-1}$ ; burden,  $\text{Tg}$ ; lifetime, days.

States is overestimated by the model. The performance of MAM3 and MAM7 in simulating  $\text{SO}_2$  and sulfate is similar for these sites in both regions. However, modeled  $\text{SO}_2$  concentrations are slightly lower in MAM7 than in MAM3 (see model mean for these sites), while modeled sulfate concentrations are higher in MAM7, especially at the European sites (by 10–20%), indicating faster conversion of  $\text{SO}_2$  to sulfate in MAM7. This is consistent with the larger aqueous-phase chemical conversion of  $\text{SO}_2$  to sulfate in MAM7 (as discussed in Sect. 3.2) due to the explicit treatment of  $\text{NH}_3$  and ammonium in MAM7. In Europe with higher  $\text{NH}_3$  concentrations than those in United States (not shown), the increase in sulfate concentrations in MAM7 is larger.

Figure 10 compares annual mean sulfate concentrations simulated at the surface from MAM3 and MAM7 with observations from an ocean network operated by the University of Miami (Prospero et al., 1989; Savoie et al., 1989, 1993; Arimoto et al., 1996). Simulated sulfate concentrations systematically underestimate the observations at these ocean sites

for both MAM3 and MAM7, probably due to too high wet removal rates, although the correlation coefficients between modeled and observed concentrations are  $\sim 0.98$ .

Figures 11–14 compare simulated annual mean BC, organic carbon (OC), and OM from MAM3 and MAM7 with those observed at the IMPROVE sites, EMEP sites, and those compiled by Liousse et al. (1996), Cooke et al. (1999) and Zhang et al. (2007). Modeled BC concentrations agree with observations reasonably well (mostly within a factor of 2) at the IMPROVE sites (Fig. 11a), while the model significantly overestimates observed OC concentrations by more than a factor of 2, especially in the Eastern US (Fig. 12a). The OC high bias is improved when the 50% SOA yield increase (Sect. S1.1.3 in the Supplement) is removed. The model underestimates observed BC and OC concentrations at the EMEP sites (Figs. 11b and 12b). Modeled OC and BC generally capture the spatial variations of the observations compiled by Liousse et al. (1996), Cooke et al. (1999) and Zhang et al. (2007). However, BC concentrations are

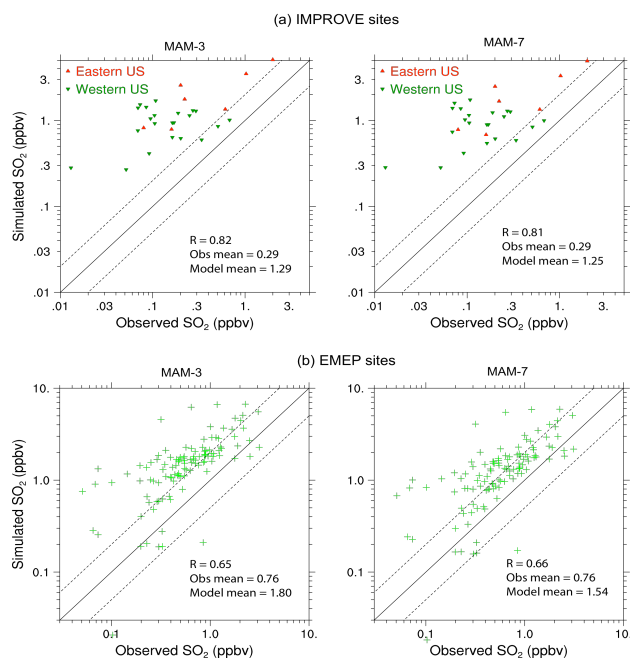


**Fig. 8.** Observed and simulated annual-average  $\text{SO}_2$  mixing ratios at IMPROVE and EMEP network sites. Observations are for site-available years between 1990–2005 for IMPROVE sites and 1995–2005 for EMEP sites. Simulated values for MAM3 (left) and MAM7 (right) are from model lowest layer. Top: IMPROVE network; Eastern US sites are east of  $97^\circ$  W longitude. Bottom: EMEP network.

significantly underestimated in remote regions and at some Pacific and Atlantic locations, suggesting too strong wet removal of BC during its transport from source regions. These results for MAM3 and MAM7 are very similar due to the hygroscopicity ( $\kappa = 0.1$ ) used for POM. Modeled OM concentrations are within a factor of 2 of observations at most sites compiled by Zhang et al. (2007).

We compare model-simulated vertical profiles of BC with aircraft measurements from several field campaigns in the tropics and subtropics, over mid-latitude North America (Fig. 15) and at high latitudes (Fig. 16). These measurements were made by a single particle soot absorption photometer (SP2) (Schwarz et al., 2006). Koch et al. (2009) gave a detailed description of aircraft flights and data processing. The observed mean as well as median and standard deviation are shown in the figures when available. Modeled BC profiles are based on monthly results interpolated to the average latitude and longitude of flight tracks. Measured BC mixing ratios show a strong gradient (by 1–2 orders of magnitude) from the boundary layer to the free troposphere in the tropics (CR-AVE and TC4) and subtropics (AVE Houston). Modeled BC mixing ratios from MAM3 and MAM7 show a smaller decrease with altitude in the free troposphere, thus overestimating observations above 600–500 hPa by a factor of 10, although the agreement is better (within the data standard

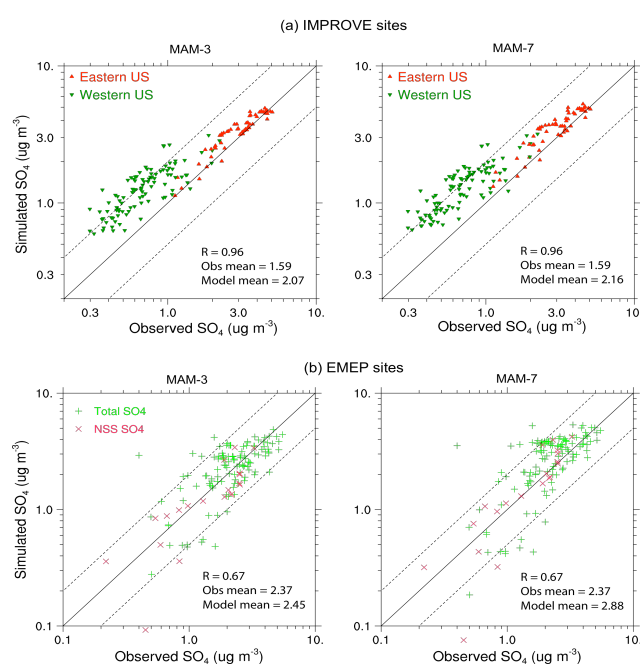


**Fig. 9.** Observed and simulated annual-average sulfate ( $\text{SO}_4$ ) concentrations at IMPROVE and EMEP network sites. Observations are for site-available years between 1995–2005. Simulated values for MAM3 (left) and MAM7 (right) are from model lowest layer. Top: IMPROVE network; Eastern US sites are east of  $97^\circ$  W longitude. Bottom: EMEP network. EMEP plots show total and non-sea salt (nss)  $\text{SO}_4$ , and IMPROVE plots show total  $\text{SO}_4$ . The CAM5  $\text{SO}_4$  species are nss- $\text{SO}_4$ , and simulated total  $\text{SO}_4$  includes a sea-salt component equal to 7.7 % of the simulated sea salt concentration. The means and correlation coefficients ( $R$ ) are for total  $\text{SO}_4$ .

deviation) in the boundary layer. This overestimation of BC mixing ratio in the free troposphere is also shown in almost all the models participating in the AeroCom project (Koch et al., 2009). We note that this high bias in the EMAC/MADE-in model was significantly reduced when the scavenging of BC by ice clouds was included (Aquila et al., 2011). The campaign in the mid-latitudes of North America (CARB) encountered strong biomass burning plumes, and BC mixing ratios show less reduction below  $\sim 700$  hPa. The modeled BC mixing ratios agree with the observed median (more representative of the background condition) better than with the observed mean.

Unlike those in the lower latitudes, observed BC mixing ratios at polar latitudes are relatively uniform up to 400 hPa, especially in spring (Fig. 16). This is due to the transport of pollutants to the Arctic from mid-latitudes by meridional lofting along isentropic surfaces. Modeled BC mixing ratios from MAM3 and MAM7 are significantly lower than those observed below 200 hPa, resulting from the too efficient wet removal of BC during its transport and/or the model's BC emissions (IPCC AR5 year 2000) missing some local fire events. This underestimation of BC below 200 hPa is also

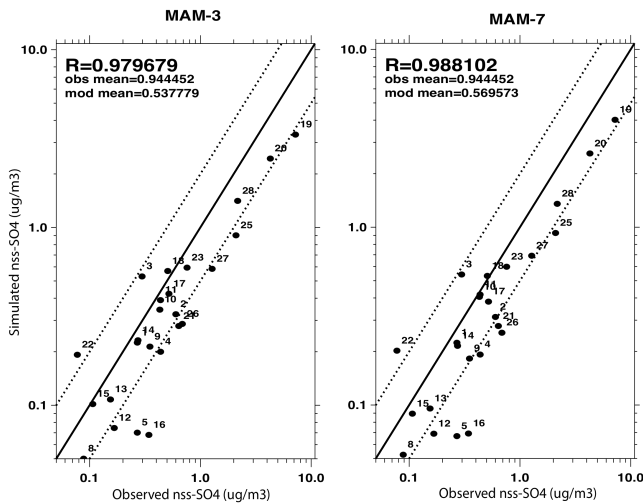


**Fig. 10.** Observed and simulated annual-average non-sea salt sulfate ( $\text{nss-SO}_4$ ) concentrations ( $\mu\text{g m}^{-3}$ ) at marine sites operated by the Rosenstiel School of Marine and Atmospheric Science (RSMAS) at the University of Miami. Observations are for site-available years between 1981–1998. Simulated values for MAM3 (left) and MAM7 (right) are from model lowest layer, and the Tenerife mountain site is not included. The global locations of sites denoted by different numbers in the figure can be found in Wang et al. (2011).

simulated by most of the AeroCom models (Koch et al., 2009). The too efficient removal of BC is related to excessive liquid clouds in the NH in CAM5.1 (H.-L. Wang, personal communication, 2011) and/or too fast wet removal of fossil fuel BC (see Sect. 5 for sensitivity tests). Therefore, although too much BC is transported to the free troposphere by convection in the lower latitudes (Fig. 15), there is much less BC arriving in the higher latitudes due to fast removal by precipitation. The comparison of modeled BC with observations is better in the summer, probably due to the better simulation of clouds then. Model results between MAM3 and MAM7 are similar due to the hygroscopic nature of POM used in the model. Sensitivity tests (MAM7-k and MAM7-aging) will be discussed in Sect. 5 to further examine the impact on modeled BC profiles.

Figure 17 compares modeled profiles of BC with SP2 measured BC mixing ratios during the HIAPER Pole-to-Pole Observations campaign (HIPPO1) conducted above the Arctic and remote Pacific from  $80^\circ\text{N}$  to  $67^\circ\text{S}$  during a two-week period in January 2009 (Schwarz et al., 2010). The observed BC profiles show significant differences between different latitude zones. Upper tropospheric BC mixing ratio is much lower (by two orders of magnitude) than that in the lower troposphere in the tropics ( $20^\circ\text{S}$  to  $20^\circ\text{N}$ ), which is consistent with observations included in Koch et al. (2010), as discussed in Fig. 15. The observed BC profiles show much less variation up to 200 hPa in both NH and SH mid-latitudes. Observed BC mixing ratio increases with altitude in the SH

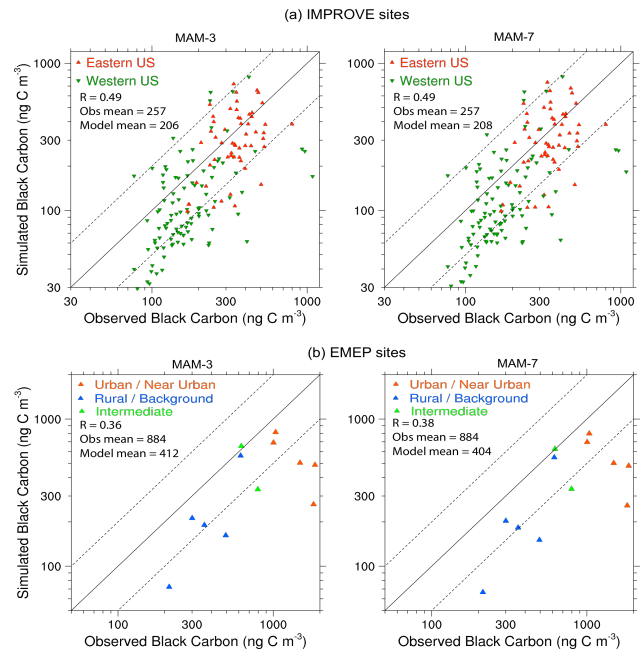


**Fig. 11.** Observed and simulated annual-average black carbon (BC) concentrations ( $\text{ng C m}^{-3}$ ) at IMPROVE and EMEP BC/OC network sites. Observations are for site-available years between 1995–2005 for IMPROVE sites and July 2002–June 2003 for EMEP sites. Simulated values for MAM3 (left) and MAM7 (right) are from model lowest layer. Top: IMPROVE network; Eastern US sites are east of  $97^\circ\text{W}$  longitude. Bottom: EMEP network.

high latitudes, reflecting the upper level transport of BC from biomass burning sources regions in South America and Southern Africa. In contrast, observed BC mixing ratio decreases with altitude in the NH high latitudes ( $60$ – $80^\circ\text{N}$ ) with very high BC mixing ratios (above  $50\text{ ng kg}^{-1}$ ) near the surface. This is different from the more uniform BC profiles observed in April (Fig. 16). MAM3 and MAM7 capture the vertical variations of BC mixing ratio reasonably well in the SH high latitudes and NH and SH mid-latitudes. However, modeled BC shows less vertical reduction in the tropics, thus significantly overestimating measurements in the upper troposphere. This overestimation is also shown in the model median and mean of AeroCom models, which is attributed to the insufficient wet removal of BC in the models by convective clouds (Schwarz et al., 2010). Similar to the results in Fig. 16 for the NH high latitudes in April, modeled BC significantly underestimates the observations below 300 hPa. There is little difference between model BC in MAM3 and MAM7, although BC mixing ratios from MAM7 are slightly higher. We will further discuss the impact of BC aging on modeled BC profiles in Sect. 5.

Figures 18 and 19 compare the simulated annual mean dust concentrations and dust deposition fluxes at the surface from MAM3 and MAM7 with observations collected by Mahowald et al. (2009). As for sulfate, dust concentrations

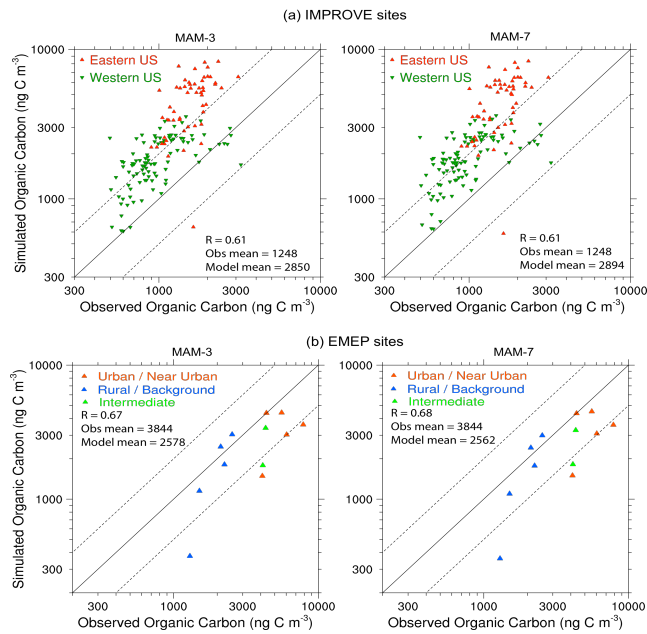


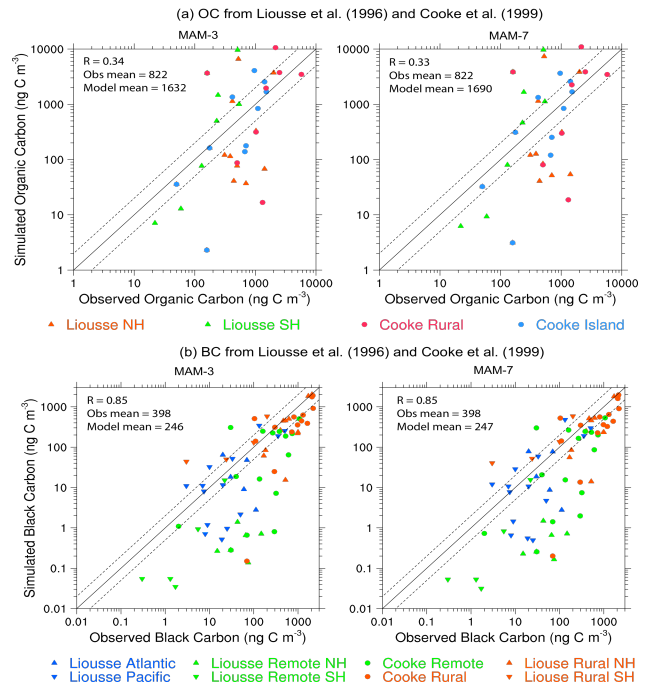
**Fig. 12.** Observed and simulated annual-average organic carbon (OC) concentrations ( $\text{ng C m}^{-3}$ ) at IMPROVE and EMEP BC/OC network sites. Observations are for site-available years between 1995–2005 for IMPROVE sites and July 2002–June 2003 for EMEP sites. Simulated values for MAM3 (left) and MAM7 (right) are from model lowest layer and are equal to the modeled (POM + SOA)/1.4. Top: IMPROVE network; Eastern US sites are east of  $97^\circ$  W longitude. Bottom: EMEP network.

are underestimated at many sites, especially in MAM3, although the simulated multi-sites means are slightly greater than observed ones. The underestimation is reduced in MAM7, which is consistent with the higher dust burden and concentration in MAM7. Modeled dust deposition fluxes are also lower than limited observational data.

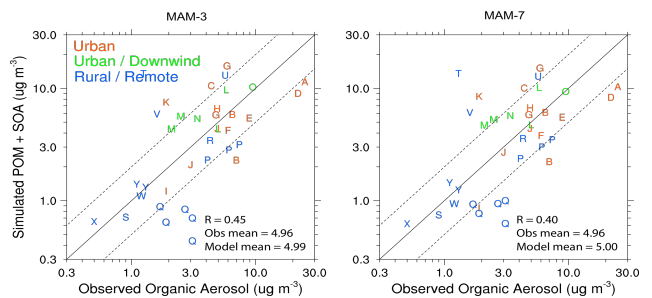
Figure 20 compares the simulated annual mean sea salt concentrations at the surface from MAM3 and MAM7, with observations obtained at the ocean sites operated by the University of Miami. Most of the simulated sea salt concentrations are within a factor of 2 of the observations, although there is large scatter between the model and observations, and correlation coefficients are low (0.23–0.25) in part due to the narrow range of the model and observed sea salt concentrations. As discussed in Sect. 3, MAM7 simulates lower sea salt concentrations compared to MAM3.

**4.2 Aerosol number concentration and size distribution**

Figure 21 compares simulated aerosol size distributions in the marine boundary layer with observations from Heintzenberg et al. (2000). The observational data were compiled and aggregated onto a  $15 \times 15^\circ$  grid. We sampled the model results over the same regions as those of the observations. Observations show bi-modal size distributions for all the

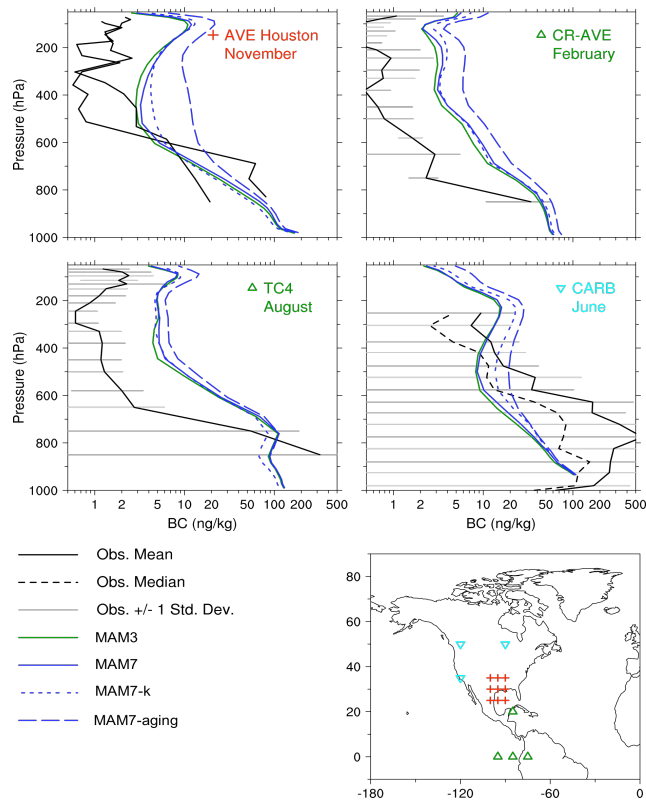


**Fig. 13.** Observed and simulated organic carbon (OC) (top) and black carbon (BC) (bottom) concentrations ( $\text{ng C m}^{-3}$ ) at various locations and time periods. Observations are from the compilations of Lioussé et al. (1996) and Cooke et al. (1999). Simulated values for MAM3 (left) and MAM7 (right) are from model lowest layer, and OC is the modeled (POM + SOA)/1.4.



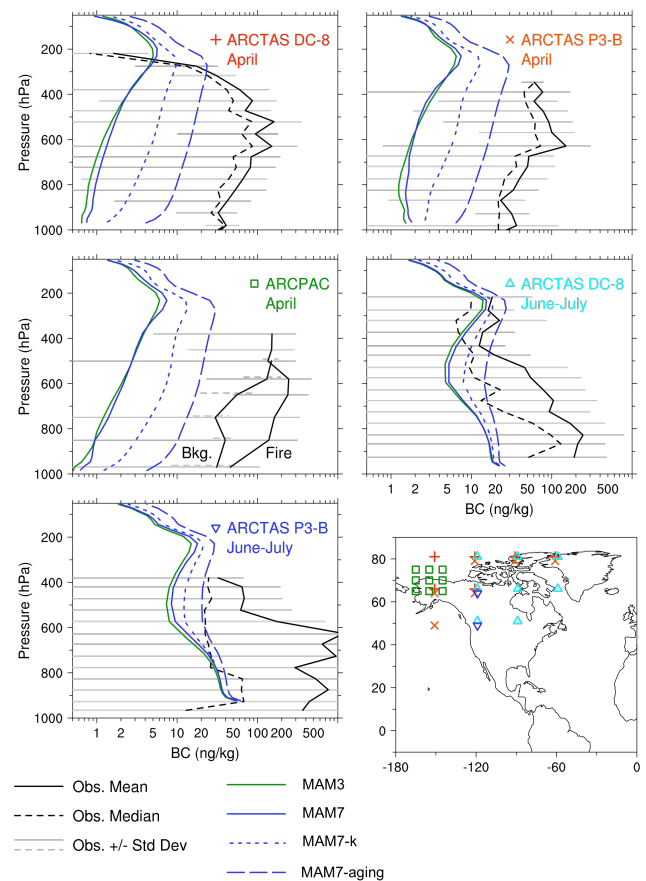
**Fig. 14.** Observed and simulated organic aerosol concentrations at various locations and times as reported and compiled by Zhang et al. (2007). Simulated values for MAM3 (left) and MAM7 (right) are from model lowest layer except for Jungfrauoch site (symbol W).

latitudinal bands, with mode median diameters of 0.03–0.06  $\mu\text{m}$  for the Aitken mode and 0.1–0.2  $\mu\text{m}$  for the accumulation mode. There are higher Aitken mode number concentrations in the SH extratropics than other latitudinal bands in the observations, probably due to stronger aerosol nucleation there. The model is able to reproduce the bi-modal size distributions. However, the model underestimates the Aitken mode number concentrations in the SH ( $15^\circ$  S– $60^\circ$  S) and NH ( $15^\circ$  N– $30^\circ$  N), which suggests that the boundary layer



**Fig. 15.** Observed and simulated BC vertical profiles in the tropics and middle latitudes from four aircraft campaigns: AVE Houston (NASA Houston Aura Validation Experiment), CR-AVE (NASA Costa Rica Aura Validation Experiment), TC4 (Tropical Composition, Cloud and Climate Coupling), and CARB (NASA initiative in collaboration with California Air Resources Board). Observations are averages for the respective campaigns and were measured by three different investigator groups: NOAA (Schwarz et al., 2006) for AVE-Houston, CR-AVE, and TC4; University of Tokyo (Moteki and Kondo, 2007; Moteki et al., 2007) and University of Hawaii (Clarke et al., 2007; Howell et al., 2006; McNaughton et al., 2009; Shinozuka et al., 2007) for CARB. The Houston campaign has two profiles from two different days. See Koch et al. (2009) for additional details. Simulated profiles for MAM3 and MAM7 are averaged over the points on the map and the indicated month. Two sensitivity experiments are included: MAM7-k and MAM7-aging, as discussed in Sect. 5.

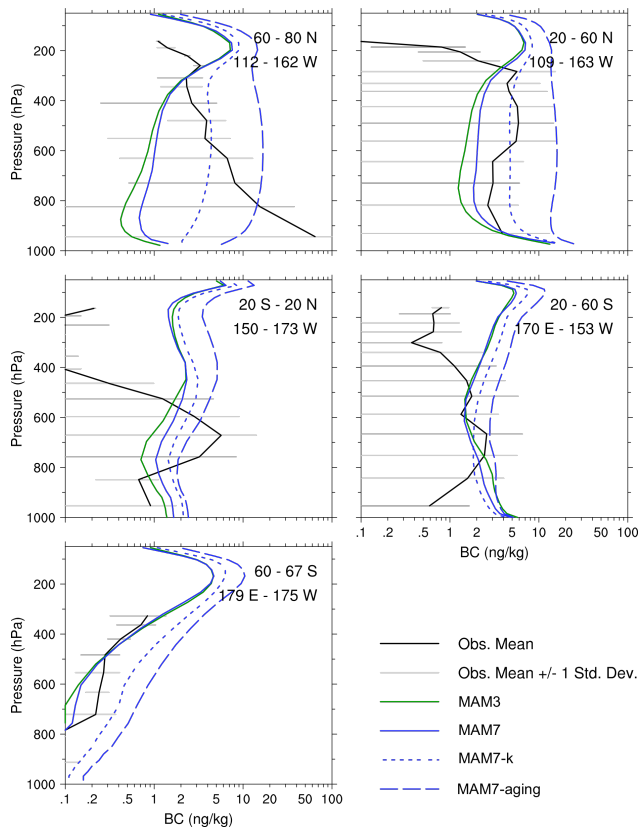
nucleation in these remote regions is too weak, the ultrafine sea salt emission flux is too small, or the model misses an organic ocean source. The results for the SH are consistent with Pierce and Adams (2006). In the NH mid-latitudes, the model underestimation of Aitken mode aerosol number concentration may also suggest that the anthropogenic influence is too weak. The model underestimates the accumulation mode number concentrations in almost all latitude bands. This suggests that the model may have too low fine sea salt emission flux, too strong wet removal of sea salt in the marine boundary layer and anthropogenic aerosols during the transport from



**Fig. 16.** Same as Fig. 15, but for BC vertical profiles at high latitudes from two other campaigns: ARCTAS (NASA Arctic Research of the Composition of the Troposphere from Aircraft and Satellite) and ARCPAC (NOAA Aerosol, Radiation, and Cloud Processes affecting Arctic Climate). Observations are from the NOAA group for ARCPAC and from the University of Tokyo and University of Hawaii groups for ARCTAS.

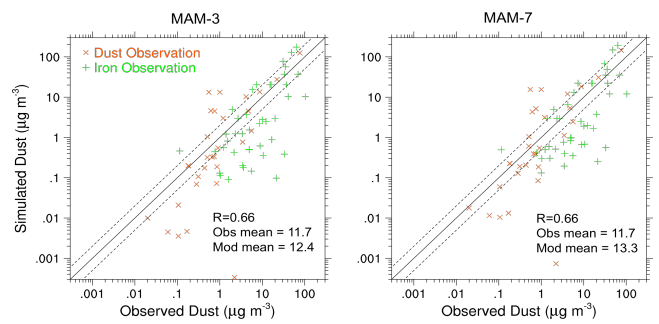
the continents, and/or missing organic source from oceans. There are higher Aitken mode aerosol number concentrations in MAM7 than those in MAM3 in all these marine zonal bands, consistent with the higher nucleation rates of aerosol in MAM7, as indicated in Sect. 3.1. The difference in the accumulation mode aerosol number concentration is small between MAM3 and MAM7.

Figure 22 compares simulated vertical profiles of aerosol number concentration for particles with diameter larger than 14 nm ( $N_{14}$ , for which the model values include particles from all modes) and particles with diameter larger than 100 nm ( $N_{100}$ , for which the model values include particles from accumulation, primary carbon, and larger modes) with observations near Punta Arena, Chile ( $53^\circ$  S) and Prestwick, Scotland ( $54^\circ$  N) during the Interhemispheric Differences in Cirrus Properties From Anthropogenic Emissions (INCA) campaign (Minikin et al., 2003). Observed  $N_{14}$  number concentrations in both locations show little variation up



**Fig. 17.** Same as Fig. 16, but for BC vertical profiles above W. Canada, Alaska, the Arctic Ocean, and the remote Pacific Ocean during the HIPER Pole-to-Pole Observations (HIPPO) campaign in January 2009 (Schwarz et al., 2010). The observational data were grouped into five latitude zones (67–60° S, 60–20° S, 20° S–20° N, 20–60° N, and 60–80° N). Simulated profiles for MAM3 and MAM7 are averaged over January and the flight track segments within each latitude zone. Two sensitivity experiments are included: MAM7-k and MAM7-aging, as discussed in Sect. 5.

to 8–10 km. The  $N_{14}$  number concentrations in Scotland are a factor of 2–3 higher than those in Chile. Modeled  $N_{14}$  number concentrations also show small vertical variations up to 10 km; however, they are similar between the two locations. The modeled concentrations are lower than those from measurements, especially at the NH location (Scotland). This underestimation may be partly due to the large assumed size of carbonaceous aerosols emitted from fossil fuel combustion and/or that the aerosol nucleation is too weak due to the too efficient removal of precursor gases (e.g.,  $SO_2$ ). Observed  $N_{100}$  number concentrations decrease significantly with height in the boundary layer, and then vary little in the middle troposphere and increase slightly around 10 km for both locations. The model captures these vertical variations well and also the much higher concentrations in the NH (Scotland) than those in the SH (Chile). The model underestimates the observed  $N_{100}$  number concentrations, especially



**Fig. 18.** Observed and simulated annual-average mineral dust concentrations ( $\mu\text{g m}^{-3}$ ). Observations are from Table S2 of Mahowald et al. (2009). Only station measurements are shown (no cruise measurements). The symbols distinguish the original data types: actual dust measurement ( $\times$ ) or dust concentration calculated from iron measurement (+), assuming 3.5% iron in dust, as in Mahowald et al. (2009).

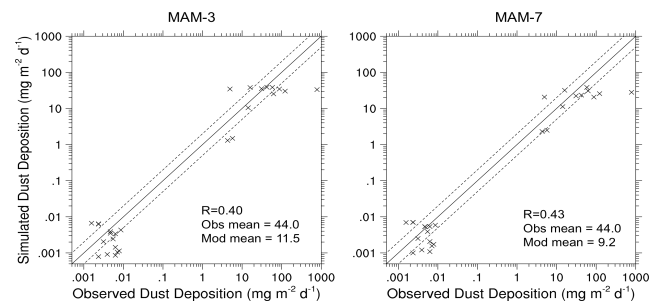


**Fig. 19.** Observed and simulated annual-average mineral dust total (dry plus wet) deposition fluxes ( $\text{mg m}^{-2} \text{d}^{-1}$ ). Observations are from Table S1 of Mahowald et al. (2009). Dust deposition fluxes were calculated from the iron deposition fluxes, assuming 3.5% iron in dust.

at the NH location (Scotland). There are slightly higher number concentrations from MAM7 than those from MAM3 for both  $N_{14}$  and  $N_{100}$  at both locations.

Figure 23 compares vertical profiles of modeled CCN number concentrations at supersaturation of 0.1% with data from the eight field experiments reported in Ghan et al. (2001). Observations show a variety of vertical profiles of CCN number concentrations. CCN number concentrations increase with altitude over Tasmania in the austral winter and over the Arctic in spring, and vary little over Tasmania during ACE-1 in the austral summer. These vertical profiles suggest the influence of continual outflows from Australia or from mid-latitudes. At other sites observed CCN number concentrations decrease with altitude. The model results show a decrease with altitude for all sites. The model severely underestimates the observed CCN number concentration in the Arctic in spring, which is consistent with the underestimation of BC concentration due to the too efficient wet scavenging in the model. The ARM site in Oklahoma is located in

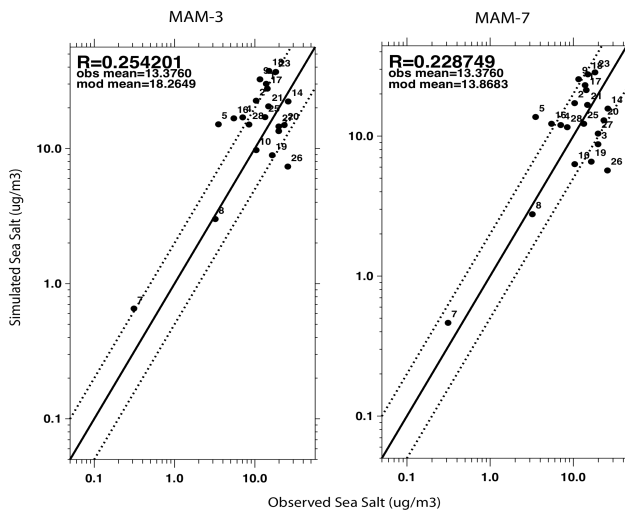


**Fig. 20.** Same as Fig. 10, but for sea salt concentrations ( $\mu\text{g m}^{-3}$ ). The global locations of sites denoted by different numbers in the figure can be found in Wang et al. (2011).

a strong concentration gradient region, and the model may not be able to accurately resolve and simulate these spatial variations. The assumed size for fossil fuel BC and POM emissions could also contribute to the underestimation of observed CCN number concentration. The model performance is qualitatively similar to that found by Wang et al. (2011) and Ghan et al. (2001). CCN number concentrations near the surface over ocean from MAM7 are significantly lower than those of MAM3, as discussed in Sect. 3.1.

### 4.3 Aerosol optical properties

Figure 24 compares the monthly aerosol optical depth (AOD) and single scattering albedo (SSA) at 550 nm from the model with observations from the AERONET (<http://aeronet.gsfc.nasa.gov>) at sites in seven regions (North and South America, Europe, East and South Asia, and Northern and Southern Africa) over the globe. The AERONET data are averaged for the years of 1998–2005. Modeled monthly AOD agrees with observations within a factor of 2 for sites in North America. The model also captures the seasonal variations of observed AOD in North America reasonably well: AOD is lower in the winter and higher in the summer due to stronger photochemical production of sulfate and stronger biogenic SOA sources in the summer (figure not shown). At several sites, the modeled AOD values are lower than observations in the summer, probably due to the too strong wet scavenging in the model. Differences in simulated AOD between MAM3 and MAM7 are small in North America. The normalized mean bias (NMB) of simulated AOD in MAM3 and MAM7 is  $-0.28$  there (Table 9). The underestimation of monthly AOD is much more severe in South and East Asia (by more than a factor of 2), probably due to the underestimation of

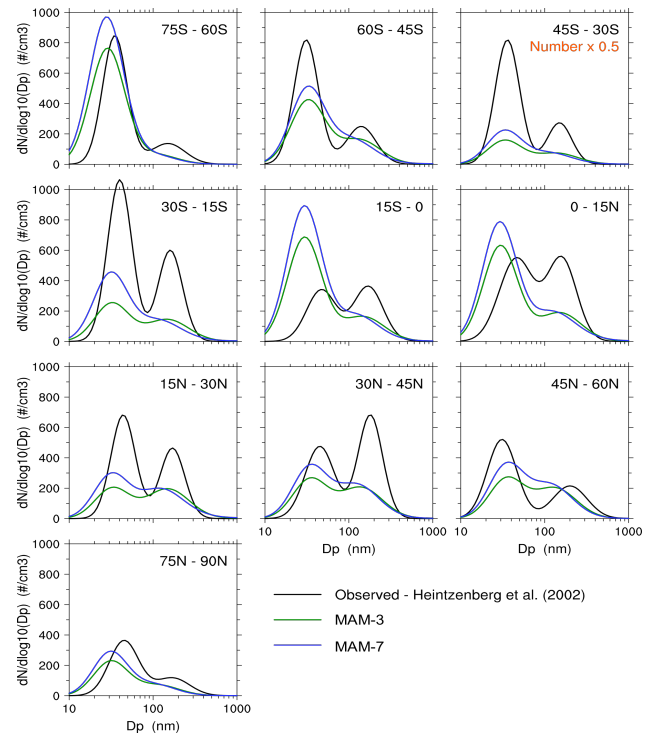


**Fig. 21.** Submicron aerosol number size distributions in the marine boundary layer. Observations (Obs.) from Heintzenberg et al. (2000) were compiled and aggregated onto a  $15 \times 15^\circ$  grid then averaged zonally. The model data are spatially averaged over the  $15 \times 15^\circ$  grid cells having observations. Model data for MAM3 and MAM7 are temporally averaged over December–February for 75–45° S, over November–March for 45–30° S, annually for 30° S–30° N, over May–September for 30–45° N, over June–August for 45–90° N. For the 45–30° S latitude band, aerosol number densities are scaled by 0.5, so the same vertical axis can be used for all latitudinal bands.

anthropogenic emissions there. The model captures well the seasonal variations of AOD in Northern Africa (figure not shown), and MAM7 has a much better simulation (NMB of  $-0.12$ ) compared to MAM3 (NMB of  $-0.37$ ), due to its higher dust burdens and concentrations (Sect. 3). In Southern Africa, the model is able to capture the AOD seasonal trends resulting from the biomass burning emission (figure not shown). However, both MAM3 and MAM7 underestimate the AOD peaks in autumn there.

The modeled SSA ranges mostly between 0.88–0.94 and has less variation than observations. This is indicated in the low correlation coefficients between model simulations and observations (Table 10). The model captures well the seasonal variations (not shown) and magnitudes of SSA in Northern and Southern Africa. The modeled SSA is lower than observations in East Asia, probably because of the underestimation of sulfate and organic aerosol there, while it is higher than observations in South America, probably because of the underestimation of local biomass burning sources

**Table 9.** Mean of observations (obs), and normalized mean bias (NMB) and correlation coefficients ( $R$ ) between model simulations and observations, for AOD over the seven regions in Fig. 24. The NMB is the difference between model and observed means divided by the observed mean.

	North America	Europe	East Asia	Northern Africa	Southern Africa	South America	South Asia	Global
Mean (obs)	0.13	0.18	0.34	0.51	0.18	0.21	0.39	0.21
NMB (MAM3)	-0.28	-0.38	-0.53	-0.37	-0.39	-0.24	-0.71	-0.33
NMB (MAM7)	-0.28	-0.38	-0.50	-0.12	-0.33	-0.29	-0.72	-0.24
$R$ (MAM3)	0.87	0.29	0.36	0.55	0.66	0.44	0.78	0.69
$R$ (MAM7)	0.87	0.28	0.31	0.51	0.49	0.50	0.80	0.71

**Table 10.** Mean of observations (obs) and model simulations, and correlation coefficients ( $R$ ) between model simulations and observations, for SSA over the seven regions in Fig. 24.

	North America	Europe	East Asia	Northern Africa	Southern Africa	South America	South Asia	Global
Mean (obs)	0.93	0.91	0.92	0.91	0.89	0.88	0.90	0.92
Mean (MAM3)	0.92	0.91	0.88	0.90	0.91	0.94	0.92	0.91
Mean (MAM7)	0.92	0.91	0.88	0.91	0.90	0.94	0.92	0.91
$R$ (MAM3)	0.28	-0.17	0.58	0.55	0.61	0.35	0.48	0.24
$R$ (MAM7)	0.31	-0.16	0.61	0.51	0.61	0.28	0.47	0.27

there. Because of the combination of the AOD and SSA, modeled absorption AOD (AAOD) is mostly within a factor of 2 of observations in North America, Europe, East Asia (due to the compensation of low AOD by low SSA), and Northern Africa for MAM7 (figure not shown). MAM3 underestimates observed AAOD in Northern Africa due to the underestimation of dust AOD. Both MAM3 and MAM7 underestimate AAOD in Southern Africa (due to the underestimation of biomass burning AOD), in South Asia (due to the underestimation of anthropogenic AOD and overestimation of SSA), and in South America (due to the overestimation of SSA).

Figure 25 shows the simulated AOD at 550 nm from MAM3 and MAM7 in January and July, in comparison with that from a satellite AOD retrieval composite derived by Kinne et al. (2006). As noted in Kinne et al. (2006), this satellite composite combines the strength of individual satellite retrievals (MODIS, MISR, AVHRR, TOMS, and POLDER), giving regional preferences for different satellite products separately over land and over ocean. The simulated AOD captures the general patterns of AOD on the global scale. The model simulates higher AOD over the biomass burning region in Southern Africa in January, in agreement with satellite data. The model underestimates satellite-observed AOD over North America, Europe and East Asia in January. The model captures the observed AOD peaks over the Saharan and Asian deserts, biomass burning regions over Southern Africa and South America, and industrial regions over East and South Asia in July. The model underestimates observed AOD in East Asia, North America and Southern

Africa in July, which agrees with the comparison of modeled AOD with the AERONET data. The model overestimates the outflow of Saharan dust and South American biomass aerosols over the central Atlantic and eastern equatorial Pacific, respectively. Modeled AOD from MAM3 and MAM7 is similar over the continents with higher AOD over Northern Africa in MAM7. Modeled AOD in MAM3 over oceans agrees reasonably well with satellite data, while modeled AOD in MAM7 is significantly lower over oceans (e.g., in the storm track regions), consistent with the lower sea salt concentrations in MAM7, as discussed in Sect. 3.

We note here that the evaluation of modeled cloud properties from MAM3 and MAM7 with available observations, which is important for the aerosol wet removal, is given in Sect. S2.1 of the Supplement.

#### 4.4 Timing

It takes about 4.8 h of wall-clock time for a one-year simulation with the stand-alone CAM5 with MAM3 (with 15 aerosol and 5 precursor gas species) using 128 CPUs on NCAR Bluefire, an IBM Power 6. It takes 6.3 h for MAM7 (with 31 aerosol and 6 trace gas species); thus, CAM5 with MAM7 is  $\sim 30\%$  slower than CAM5 with MAM3. The wall-clock time for running MAM3 is  $\sim 35\%$  higher than that using the CAM5 with the prognostic bulk aerosol module (BAM, with 13 aerosol and 3 precursor gas species). This increase in computational time is due to the additional aerosol microphysics processes (e.g., nucleation, condensation, coagulation) considered in MAM3.

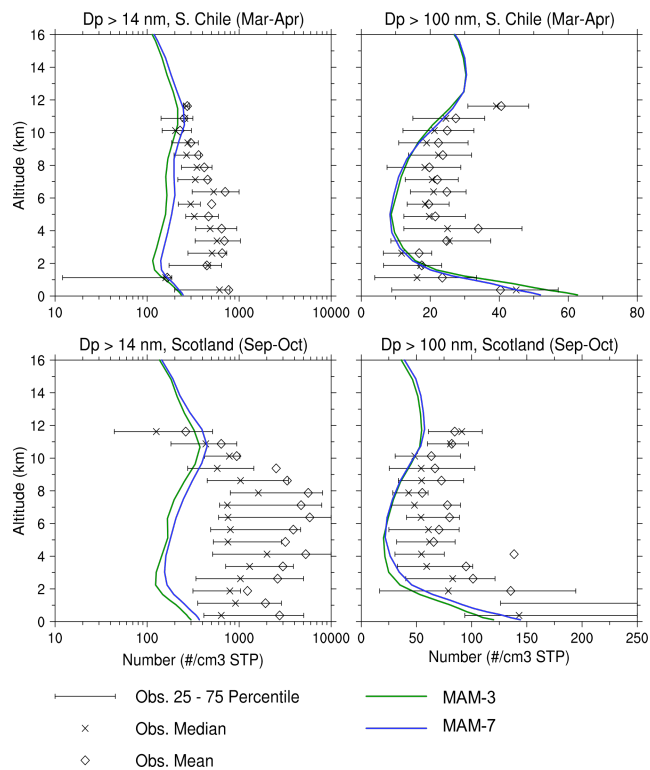


**Fig. 22.** Vertical profiles of aerosol number concentration of particles with diameter  $> 14$  nm (left) and particles with diameter  $> 100$  nm (right), near Punta Arenas, Chile during March/April (top) and near Prestwick, Scotland in September/October (bottom). Observations are from Minikin et al. (2003): median (star), 25 and 75 percentiles (left and right end of error bars). Model results for MAM3 and MAM7 are averaged over latitude-longitude ranges of  $60\text{--}50^\circ$  S,  $70\text{--}85^\circ$  W for Chile, and over  $50\text{--}60^\circ$  N,  $10^\circ$  W– $5^\circ$  E for Scotland.

## 5 Sensitivity studies

In the standard MAM7 (MAM7-control) the hygroscopicity ( $\kappa$ ) value for POM is 0.1. As a result POM and BC in the primary carbon mode experience wet scavenging before aerosol particles in the primary carbon mode are aged into the accumulation mode. Therefore, we do not find large differences in model-simulated POM and BC between MAM7 and MAM3. In one sensitivity experiment the  $\kappa$  value of POM is changed from 0.1 to 0.0 to reflect the non-hygroscopic nature ( $\kappa = 0$ ) of POM from fossil fuel combustion. We run MAM7 to examine the impact of this change on model-simulated POM and BC (experiment MAM7-k). In another sensitivity experiment, in addition to  $\kappa = 0$  for POM we change the coating criterion for conversion of POM and BC in the primary carbon mode to accumulation mode. The coating thickness is changed from 3 to 8 monolayers. Thus, more coating material (sulfate, ammonium and SOA) is required to age primary carbon mode particles and transfer them to the accumulation mode (experiment MAM7-aging). For a

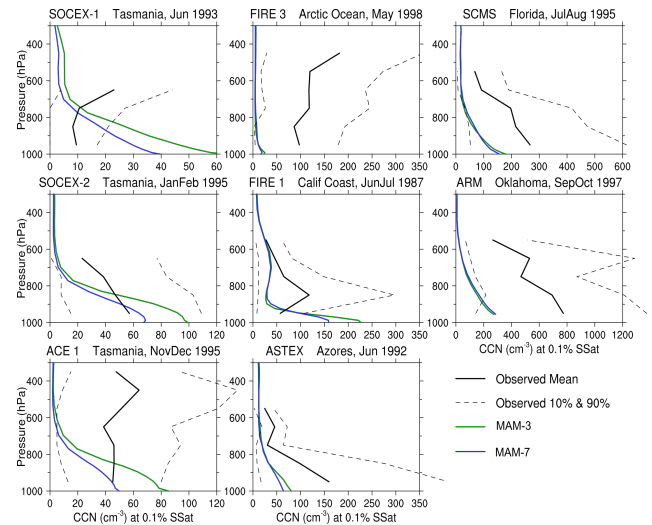


**Fig. 23.** Observed and simulated vertical profiles of CCN concentrations at 0.1 % supersaturation for eight field experiments. Field experiment acronym, location, and date are shown above each plot, and more details are given in Table 1 of Ghan et al. (2001). Observed values are means (solid black lines) and 10th and 90th percentiles (dashed black lines) for each experiment. Simulated values (colored lines) for MAM3 and MAM7 are averages over the months shown and experiment location.

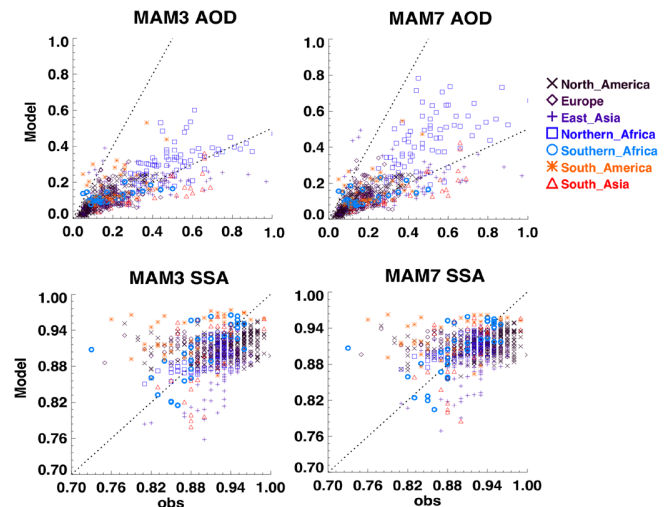


**Fig. 24.** Comparison of modeled monthly aerosol optical depth (AOD) (upper) and single scattering albedo (SSA) (lower) at 550 nm from MAM3 (left) and MAM7 (right) with observations from the AERONET (<http://aeronet.gsfc.nasa.gov>) at 75 sites in seven regions (North and South America, Europe, East and South Asia, and Northern and Southern Africa) over the globe. Dashed lines are 1:2 or 2:1 for AOD (upper) and 1:1 for SSA (lower).

$0.134\text{ }\mu\text{m}$  diameter non-hygroscopic particle, which is the volume-mean size for BC and POM emissions, the 3 and 8 monolayers of sulfate produce CCN with critical supersaturations of 0.49 % and 0.32 %, respectively.

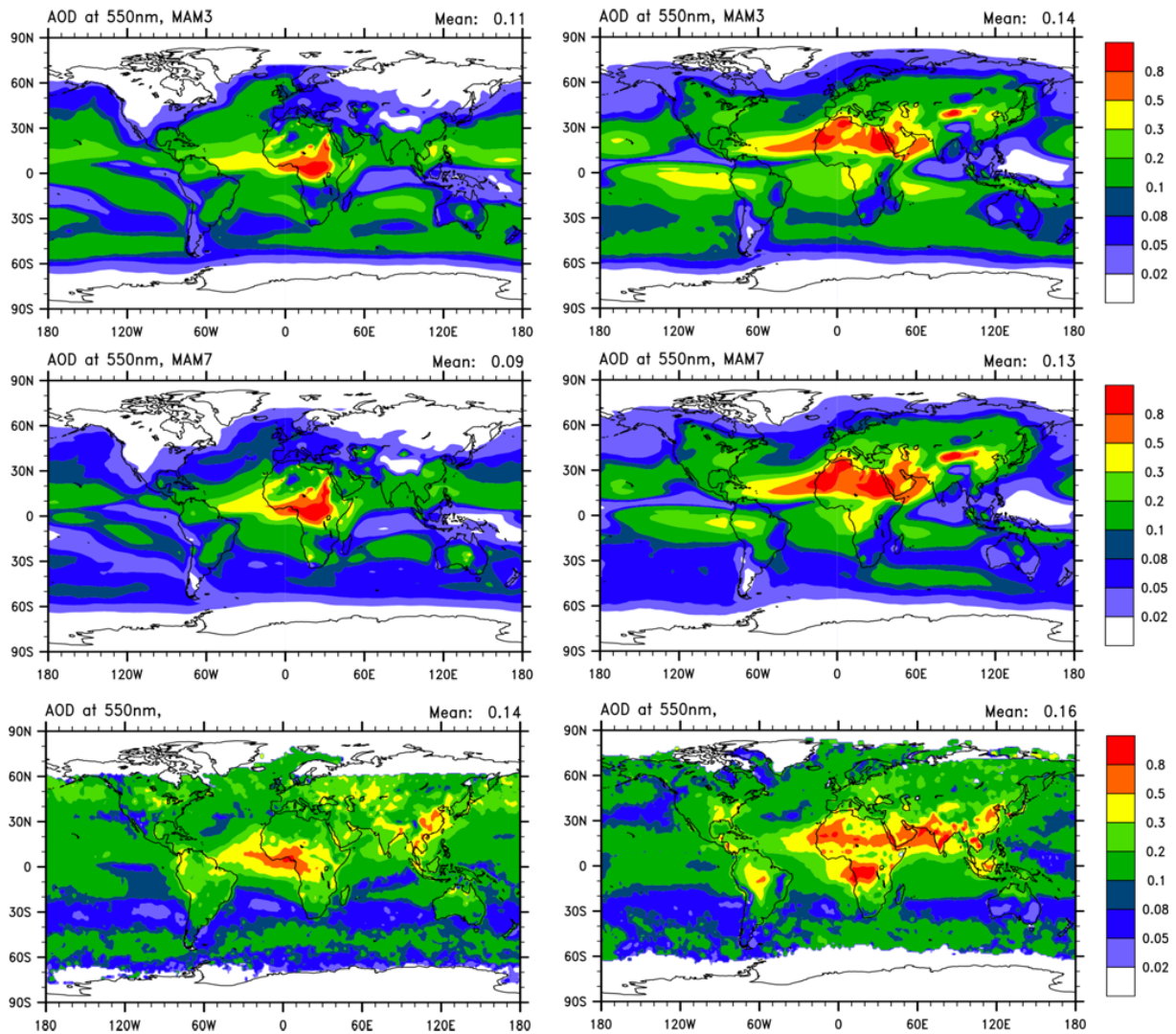


**Fig. 25.** Comparison of simulated AOD at 550 nm from MAM3 (upper) and MAM7 (middle) in January (left) and July (right) with that from a satellite AOD retrieval composite (lower), derived by Kinne et al. (2006).

Tables 11 and 12 give the global budgets of POM and BC, respectively from the two sensitivity experiments (MAM7-k and MAM7-aging) in comparison with those from the MAM7-control experiment. In the MAM7-k experiment, when droplet activation and in-cloud scavenging are suppressed by the lower value of  $\kappa$ , the global POM and BC burdens in the primary carbon mode increase by  $\sim 40\%$ , and their lifetimes are thus longer. With less wet removal in the primary carbon mode, more POM and BC are transferred to the accumulation mode. Once in the accumulation mode, they experience the same dry and wet removal efficiencies as those in MAM7-control. Thus, burdens of POM and BC in the accumulation mode are higher but with similar lifetimes as MAM7-control. The global burdens of total POM and BC (i.e., primary carbon mode plus accumulation mode)

in MAM7-k are 10% and 8% higher than those in MAM7-control, respectively.

With slower aging and less wet removal in the primary carbon mode (MAM7-aging), global burdens of POM and BC in the primary carbon mode increase by a factor of  $\sim 4$ , with much longer lifetimes than those in MAM7-control. Similar amounts of POM and BC are transferred to the accumulation mode as in MAM7-control as a result of less wet removal but more dry deposition (due to the slower aging) in the primary carbon mode. POM and BC burdens and lifetimes in accumulation mode are similar to those in MAM7-control. The global burdens of total POM and BC in MAM7-aging are 43% and 34% higher than those in MAM7-control, respectively.

A reduced  $\kappa$  value for POM and slower aging of primary carbon mode produce small changes for POM and

**Table 11.** Global budgets for primary carbon mode and accumulation mode POM from the standard MAM7 simulation (MAM7-control) and the MAM-k and MAM-aging sensitivity experiments.

	MAM7-control	MAM7-k	MAM7-aging
Primary carbon mode POM			
Sources	50.2	50.2	50.2
Fossil and bio-fuel emission	16.8	16.8	16.8
Biomass burning emission	33.4	33.4	33.4
Sinks	50.2	50.2	50.2
Dry deposition	2.5	2.8	4.5
Wet deposition	2.6	0.004	0.009
Aged to accumulation mode	45.1	47.4	45.7
Burden	0.10	0.14	0.37
Lifetime	0.73	1.0	2.7
Accumulation mode POM			
Sources			
Aged from primary mode	45.1	47.4	45.7
Sinks	44.9	47.3	45.6
Dry deposition	5.8	6.1	5.5
Wet deposition	39.1	41.2	40.1
Burden	0.58	0.61	0.60
Lifetime	4.7	4.7	4.8

Units are sources and sinks,  $\text{Tg yr}^{-1}$ ; burden, Tg; lifetime, days.

**Table 12.** Global budgets for primary carbon mode and accumulation mode BC from the standard MAM7 simulation (MAM7-control) and the MAM7-k and MAM7-aging sensitivity experiments.

	MAM7-control	MAM7-k	MAM7-aging
Primary carbon mode BC			
Sources	7.76	7.76	7.76
Fossil and bio-fuel emission	5.00	5.00	5.00
Biomass burning emission	2.76	2.76	2.76
Sinks	7.76	7.76	7.76
Dry deposition	0.39	0.42	0.70
Wet deposition	0.33	0.00	0.00
Aged to accumulation mode	7.04	7.34	7.06
Burden	0.010	0.014	0.040
Lifetime	0.47	0.66	1.88
Accumulation mode BC			
Sources			
Aged from primary mode	7.04	7.34	7.06
Sinks	7.03	7.32	7.05
Dry deposition	1.02	1.04	0.93
Wet deposition	6.01	6.28	6.12
Burden	0.083	0.086	0.085
Lifetime	4.3	4.3	4.4

Units are sources and sinks,  $\text{Tg yr}^{-1}$ ; burden, Tg; lifetime, days.

BC surface concentrations near the continental source regions (e.g., at the IMPROVE and EMEP sites) in comparison with MAM7-control (figures not shown), indicating the lower sensitivity of aerosol concentrations to the difference

in wet removal near the sources (Liu et al., 2007). However, the underestimations of POM and BC surface concentrations at ocean and remote continental sites in MAM7-control are improved, especially for BC (figure not shown). The impact

on vertical profiles of BC mixing ratio from the two sensitivity experiments is shown in Figs. 15–17. With a reduced  $\kappa$  value for POM (MAM7-k experiment), BC mixing ratios are increased in comparison with MAM7-control due to less efficient wet scavenging of BC in the primary carbon mode. However, the increases are small in the tropics and subtropics in North America (Fig. 15). There are significant increases in the BC mixing ratios in the upper troposphere in the mid-latitudes (during the CARB campaign in June). BC mixing ratios are enhanced several fold in the Arctic during spring, when the control-run mixing ratios are very low, but less so in the summer, when control-run mixing ratios are higher (Fig. 16). These changes are consistent with the HIPPO comparison (Fig. 17), where strong increases occur in the mid- and high latitudes of NH and in the high latitudes of SH. These increases in BC mixing ratios improve model comparison with observations, except in the tropics and subtropics where the model high biases in the upper troposphere are larger.

With slower aging of primary carbon mode and  $\kappa = 0$  for POM (MAM7-aging run), increases in BC mixing ratios are evident in all the profiles of Figs. 15–17. This makes the overestimations of BC mixing ratios in the free troposphere in the tropics and subtropics even more severe. The model still underestimates observed BC median mixing ratios in the Arctic in spring, which suggests a model bias of wet scavenging for the accumulation mode aerosol and/or underestimated local emissions in the model during the spring season. The impacts of the changes from these two sensitivity experiments are small for aerosol number and size distributions over the oceans and CCN number concentrations in Figs. 21–23 (results shown only for control runs).

Figure 26 shows the fraction of the total BC column burden that is in the primary carbon mode from the three experiments: MAM7-control, MAM7-k and MAM7-aging. In the MAM7-control run, fresh BC (from fossil fuel, bio-fuel, and biomass burning emissions) is aged to the accumulation mode quickly, e.g., in the industrial regions where sulfate concentrations are high. Primary carbon mode BC fractions are 30–50 % in the tropical and boreal biomass burning source regions (e.g., Central Africa, the maritime continent, and Siberia). Other than these regions aged BC dominates the total BC burden (aged fractions larger than 90 %). With reduced  $\kappa$  value for POM (MAM7-k), primary carbon mode BC fractions increase because of less wet removal. Primary carbon mode BC fractions are 30–40 % over the Arctic regions because of more transport of un-aged BC from the source regions (e.g., Siberia). These results are in general agreement with observations that carbonaceous aerosol particles are internally mixed with sulfate and other components except near the source regions (e.g., Posfai et al., 2003; Clarke et al., 2004; Moffet and Prather, 2009; Wang et al., 2010). When the high coating criterion is used for aging (MAM7-aging), primary carbon mode BC fraction increases significantly with values of 50–70 % over the Arctic

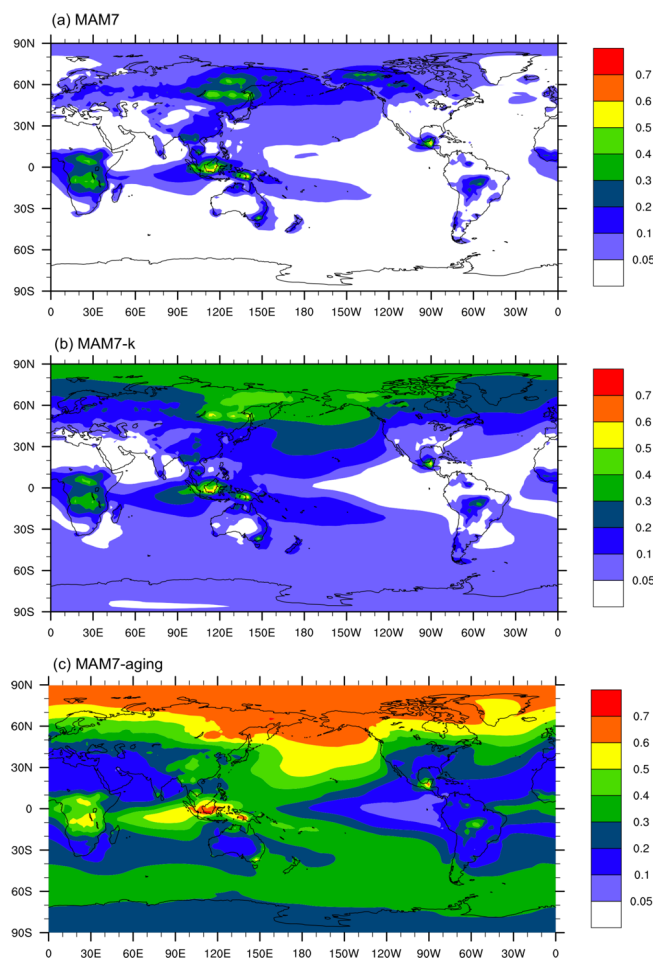


**Fig. 26.** Mass fraction of the total BC column burden that is in the primary carbon mode from the three experiments: MAM7, MAM7-k and MAM7-aging.

and biomass burning regions in the maritime continent and Central Africa. There are high fractions (30–40 %) of primary carbon mode BC in the SH mid-latitudes due to the transport from SH biomass burning regions. However, BC concentrations there are small. Evaluation of the modeled mixing state of BC and POM with observations (e.g., Pratt and Prather, 2010) will be conducted in a future study.

## 6 Conclusions and future work

In this study, the two versions of a modal aerosol module (MAM) developed for CAM5 are described and evaluated. The more comprehensive one (MAM7) has 7 log-normal modes and explicitly treats the aging of POM and BC from the primary carbon mode into which they are emitted to the accumulation mode where they are mixed with other aerosol species. For long-term (decades to centuries) simulations, a simplified version (MAM3) was developed that has 3 log-normal modes and neglects the aging process of POM and

BC by assuming the immediate mixing of POM and BC with other aerosol species. Other approximations in MAM3 include merging of the MAM7 fine dust and fine sea salt modes into the accumulation mode in MAM3, and merging of the MAM7 coarse dust and coarse sea salt modes into the single coarse mode in MAM3, which is made feasible by the separate geographical sources of sea salt and mineral dust.

Sulfate and SOA burdens and concentrations are remarkably similar between MAM3 and MAM7, because most (~90%) of these aerosol species are in the accumulation mode. Although POM and BC are treated differently in MAM3 and MAM7, POM and BC concentrations are also similar. This is because a hygroscopicity ( $\kappa$ ) of 0.1 is assumed for POM, and therefore much of the POM and BC in the primary carbon mode is wet-scavenged before aging into the accumulation mode in MAM7. Sensitivity tests with MAM7 with a lower  $\kappa$  value (0.0) for POM and additionally with a higher coating criteria for aging produce significantly larger POM and BC concentrations, especially at NH high latitudes.

Sea salt concentrations simulated by MAM7 are significantly lower (by 30–40%) over the Southern Ocean than those from MAM3, along with a lower AOD. This is primarily due to differences in the treatment of coarse-mode sea salt. MAM7 has different standard deviations ( $\sigma_g$ ) for the coarse sea salt (2.0) and dust modes (1.8), while in MAM3 the value of 1.8 is used for the single coarse mode. Thus, the coarse-mode sea salt in MAM7 has larger sedimentation velocities than those in MAM3. Also, merging MAM7 fine sea salt and accumulation modes into the MAM3 accumulation mode changes the size distribution of these submicron particles. As a result, simulated CCN number concentration (at  $S = 0.1\%$ ) and AOD from MAM7 over the oceans are lower than those from MAM3. Dust concentrations from MAM3 are slightly lower (by ~10%) than those from MAM7 due to the different size ranges for fine and coarse dust, and to a lesser extent due to the different assumptions of mixing states of dust with other components. Results from additional sensitivity tests are needed to more precisely explain how differing assumptions in MAM3 and MAM7 affect fine and coarse sea salt and dust concentrations, CCN, and AOD.

Another difference between MAM3 and MAM7 is that ammonia/ammonium cycles are explicitly treated in MAM7, but not in MAM3.  $\text{NH}_3$  dissolved in cloud water raises pH and increases aqueous-phase sulfate production. The  $\text{NH}_4/\text{SO}_4$  molar ratio in aerosol predicted in MAM7 averages 1.2 globally. It is near 2.0 in much of the continental and tropical marine boundary layer, while it is less than 1.0 in many mid-latitude marine boundary layer regions. The ratio is generally less than 1.0 in the free troposphere, except in the tropics where the ratio can be 1.5–2.0. In comparison, MAM3 assumes a fixed  $\text{NH}_4/\text{SO}_4$  molar ratio of 1.0.

Overall, the CAM5 model with MAM3 and MAM7 performs reasonably well in capturing observed spatial and temporal variations of mass concentrations of aerosol species,

aerosol number and size distribution, AOD, SSA, and CCN number concentration. There are biases in modeled aerosol fields that need to be improved in future work. Some of these biases are related to the model treatment of aerosol processes and properties, and some are related to the model treatment of cloud and other physical processes. The simulated aerosol distributions and life cycles are tightly coupled with and affected by modeled cloud fields (e.g., cloud water content, cloud cover, precipitation) in GCMs. This is expected since wet removal is the primary removal process for submicron aerosol particles, and most sulfate is formed by cloud chemistry. The cloud liquid water path simulated by CAM5 has a low bias, as indicated in Sect. S2.1 of the Supplement, but surface precipitation rates are in better agreement with observations. As a result, cycling of cloud water (i.e., conversion to precipitation) is too rapid in the model, and in-cloud wet-removal rates of aerosols are high. Simulated sulfate and mineral dust concentrations at the surface are lower than those observed at the oceanic sites operated by the RSMAS at the University of Miami. Simulated accumulation mode number concentrations are lower than those observed in the marine boundary layer by Heintzenberg et al. (2000). There is a low bias in AOD on the global scale. In addition to cloud liquid water content, the high bias in low-level cloud amount at high latitudes in cold seasons increases the occurrence of wet removal of aerosol during its transport from the mid-latitudes to the polar regions (H. Wang, personal communication, 2011). This contributes to the significantly low BC concentrations in the Arctic compared to observations from the ARCTAS and ARCPAC campaigns in April and from the HIPPO campaign in January. BC concentrations in the free troposphere in the tropics and in the mid-latitudes are, however, overestimated in the model, which suggests the need for improvement of transport and wet scavenging by convective clouds in the model. Currently, CAM5 has very simple cloud microphysics and no explicit treatment of aerosol activation in convective clouds, as well as separate (although weakly coupled) treatments of convective transport and scavenging. A more integrated treatment of the aerosol transport and scavenging by convective clouds is being developed, and the implementation of a double-moment cloud microphysics parameterization for deep convective clouds in CAM5 (Song and Zhang, 2011) will allow further improvement of aerosol processes in convective clouds.

Another source of uncertainty is aerosol emissions. Our results suggest underestimation of anthropogenic emissions in the developing countries (e.g., in East and South Asia), and biomass burning emissions in some tropical regions (e.g., in Southern Africa and South America) and boreal forest regions, which results in the low bias of simulated AOD in comparison with the AERONET and satellite data. Currently, MAM does not differentiate the properties of POM and BC between biomass burning and fossil fuel combustion sources, and it uses the same emitted size (0.134  $\mu\text{m}$  diameter) for these two, although sizes of fossil fuel-emitted particles can

be much smaller (Dentener et al., 2006). This may partially explain the too low Aitken mode number concentrations over Scotland compared with the INCA observations. Future improvement of MAM will separate POM and BC by sources with different physical and chemical properties. In addition to emissions, aerosol nucleation and growth play key roles in the aerosol number and size distribution. The model underestimation of Aitken mode number concentration in the marine boundary layer suggests needed improvement of boundary layer aerosol nucleation and the role of organics and amines from biological sources in the nucleation and growth.

Surface-level organic aerosol concentrations are overestimated in the model compared to the data obtained at the North America IMPROVE network sites (especially in the Eastern US), while model-simulated organic aerosol agrees with observations from Zhang et al. (2007) in most global sites within a factor of 2 and also with EMEP observations. The Eastern US high bias may reflect a different mixture of SOA precursors (from anthropogenic and biogenic sources), and there is better agreement when lower SOA yields are used. Future improvement of SOA formation, partitioning and aging is needed.

Nitrate, which is not treated in MAM because of its computational expense, can be important on regional scales (e.g., in East Asia) (Gao et al., 2011), and nitrate is expected to be more important in the future with the expected increase of nitrogen-oxides emissions and reduction of sulfur dioxide emissions. This can be realized through the MOSAIC (Model for Simulating Aerosol Interactions and Chemistry) (Zaveri et al., 2008) aerosol thermodynamics model, which is being implemented in CAM5. MOSAIC can also treat the water uptake of aerosol particles more accurately and include aerosol-phase chemistry during the aging process (e.g., the heterogeneous chemistry on the surface of dust particles).

Along with the above planned improvements for MAM, future work will quantify model sensitivity to approximations on aerosol modal parameters (size range and geometric standard deviation), aerosol mixing state, internal structure and shape, aerosol production, transformation, and loss processes, and climate forcing mechanisms.

**Supplementary material related to this article is available online at: <http://www.geosci-model-dev.net/5/709/2012/gmd-5-709-2012-supplement.pdf>.**

*Acknowledgements.* X. Liu, R. C. Easter, S. J. Ghan were funded by the US Department of Energy, Office of Science, Scientific Discovery through Advanced Computing (SciDAC) program. We thank M. Wang for providing the scripts for plotting some figures in this paper and J. P. Schwarz for providing the HIPPO BC data. A. Ekman would like to acknowledge the support from the Bert Bolin Center for Climate Research. M. J. Iacono was supported

by the Office of Biological and Environmental Research of the US Department of Energy under Grant No. DE-FG02-92ER61549. The CESM project is supported by the National Science Foundation and the Office of Science (BER) of the US Department of Energy. Computing resources were provided by the Climate Simulation Laboratory at NCAR's Computational and Information Systems Laboratory (CISL), sponsored by the National Science Foundation and other agencies. The Pacific Northwest National Laboratory is operated for DOE by Battelle Memorial Institute under contract DE-AC06-76RLO 1830.

Edited by: A. Stenke

## References

- Adachi, K. and Buseck, P. R.: Internally mixed soot, sulfates, and organic matter in aerosol particles from Mexico City, *Atmos. Chem. Phys.*, 8, 6469–6481, doi:10.5194/acp-8-6469-2008, 2008.
- Adachi, K., Chung, S., and Buseck, P.: Shapes of soot aerosol particles and implications for global climate, *J. Geophys. Res.-Atmos.*, 115, D15206, doi:10.1029/2009JD012868, 2010.
- Adams, P. J. and Seinfeld, J. H.: Predicting global aerosol size distributions in general circulation models, *J. Geophys. Res.*, 107, 4370, doi:10.1029/2001JD001010, 2002.
- Aquila, V., Hendricks, J., Lauer, A., Riemer, N., Vogel, H., Baumgardner, D., Minikin, A., Petzold, A., Schwarz, J. P., Spackman, J. R., Weinzierl, B., Righi, M., and Dall'Amico, M.: MADE-in: a new aerosol microphysics submodel for global simulation of insoluble particles and their mixing state, *Geosci. Model Dev.*, 4, 325–355, doi:10.5194/gmd-4-325-2011, 2011.
- Arimoto, R., Duce, R. A., Savoie, D. L., Prospero, J. M., Talbot, R., Cullen, J. D., Tomza, U., Lewis, N. F., and Jay, B. J.: Relationships among aerosol constituents from Asia and the North Pacific during PEM-West A, *J. Geophys. Res.*, 101, 2011–2023, 1996.
- Bauer, S. E., Wright, D. L., Koch, D., Lewis, E. R., McGraw, R., Chang, L.-S., Schwartz, S. E., and Ruedy, R.: MATRIX (Multiconfiguration Aerosol TRacker of mIXing state): an aerosol microphysical module for global atmospheric models, *Atmos. Chem. Phys.*, 8, 6003–6035, doi:10.5194/acp-8-6003-2008, 2008.
- Clarke, A. D., Shinozuka, Y., Kapustin, V. N., Howell, S., Huebert, B., Doherty, S., Anderson, T., Covert, D., Anderson, J., Hua, X., Moore, K. G., McNaughton, C., Carmichael, G., and Weber, R.: Size distributions and mixtures of dust and black carbon aerosol in Asian outflow: Physiochemistry and optical properties, *J. Geophys. Res.*, 109, D15S09, doi:10.1029/2003JD004378, 2004.
- Clarke, A. D., McNaughton, C., Kapustin, V., Shinozuka, Y., Howell, S., Dibb, J., Zhou, J., Anderson, B., Brekhovskikh, V., Turner, H., and Pinkerton, M.: Biomass burning and pollution aerosol over North America: Organic components and their influence on spectral optical properties and humidification response, *J. Geophys. Res.*, 112, D12S18, doi:10.1029/2006jd007777, 2007.
- Cooke, W. F., Liousse, C., Cachier, H., and Feichter, J.: Construction of a 1 degrees × 1 degrees fossil fuel emission data set for carbonaceous aerosol and implementation and radiative impact in the ECHAM4 model, *J. Geophys. Res.*, 104, 22137–22162, 1999.

- Dentener, F., Kinne, S., Bond, T., Boucher, O., Cofala, J., Generoso, S., Ginoux, P., Gong, S., Hoelzemann, J. J., Ito, A., Marelli, L., Penner, J. E., Putaud, J.-P., Textor, C., Schulz, M., van der Werf, G. R., and Wilson, J.: Emissions of primary aerosol and precursor gases in the years 2000 and 1750 prescribed data-sets for AeroCom, *Atmos. Chem. Phys.*, 6, 4321–4344, doi:10.5194/acp-6-4321-2006, 2006.
- Easter, R. C., Ghan, S. J., Zhang, Y., Saylor, R. D., Chapman, E. G., Laulainen, N. S., Abdul-Razzak, H., Leung, L. R., Bian, X., and Zaveri, R. A.: MIRAGE: Model description and evaluation of aerosols and trace gases, *J. Geophys. Res.-Atmos.*, 109, D20210, doi:10.1029/2004jd004571, 2004.
- Emmons, L. K., Walters, S., Hess, P. G., Lamarque, J.-F., Pfister, G. G., Fillmore, D., Granier, C., Guenther, A., Kinnison, D., Laepple, T., Orlando, J., Tie, X., Tyndall, G., Wiedinmyer, C., Baughcum, S. L., and Kloster, S.: Description and evaluation of the Model for Ozone and Related chemical Tracers, version 4 (MOZART-4), *Geosci. Model Dev.*, 3, 43–67, doi:10.5194/gmd-3-43-2010, 2010.
- Farina, S. C., Adams, P. J., and Pandis, S. N.: Modeling global secondary organic aerosol formation and processing with the volatility basis set: Implications for anthropogenic secondary organic aerosol, *J. Geophys. Res.*, 115, D09202, doi:10.1029/2009JD013046, 2010.
- Feng, Y. and Penner, J. E.: Global modeling of nitrate and ammonium: Interaction of aerosols and tropospheric chemistry, *J. Geophys. Res.*, 112, D01304, doi:10.1029/2005JD006404, 2007.
- Flanner, M. G., Zender, C. S., Randerson, J. T., and Rasch, P. J.: Present-day climate forcing and response from black carbon in snow, *J. Geophys. Res.-Atmos.*, 112, D11, doi:10.1029/2006jd008003, 2007.
- Forster, P., Ramaswamy, V., Artaxo, P., Bernsten, T., Betts, R., Fahey, D. W., Haywood, J., Lean, J., Lowe, D. C., Myhre, G., Nganga, J., Prinn, R., Raga, G., Schulz, M., and Van Dorland, R.: Changes in atmospheric constituents and in radiative forcing, in: *Climate Change 2007: The Physical Science Basis*, Contribution of Working Group I to the Fourth Assessment Report of the Intergovernmental Panel on Climate Change, edited by: Solomon, S., Qin, D., Manning, M., Chen, Z., Marquis, M., Averyt, K. B., Tignor, M., and Miller, H. L., Cambridge University Press, New York, 2007.
- Gao, Y., Liu, X., Zhao, C., and Zhang, M.: Emission controls versus meteorological conditions in determining aerosol concentrations in Beijing during the 2008 Olympic Games, *Atmos. Chem. Phys.*, 11, 12437–12451, doi:10.5194/acp-11-12437-2011, 2011.
- Gent, P. R., Yeager, S. G., Neale, R. B., Levis, S., and Bailey, D. A.: Improvements in a half degree atmosphere/land version of the CCSM, *Clim. Dynam.*, 79, 25–58, doi:10.1007/s00382-009-0614-8, 2009.
- Ghan, S. J. and Easter, R. C.: Impact of cloud-borne aerosol representation on aerosol direct and indirect effects, *Atmos. Chem. Phys.*, 6, 4163–4174, doi:10.5194/acp-6-4163-2006, 2006.
- Ghan, S. J. and Schwartz, S. E.: Aerosol properties and processes – A path from field and laboratory measurements to global climate models, *B. Am. Meteorol. Soc.*, 88, 1059–1083, doi:10.1175/Bams-88-7-1059, 2007.
- Ghan, S. J., Easter, R. C., Chapman, E. G., Abdul-Razzak, H., Zhang, Y., Leung, L. R., Laulainen, N. S., Saylor, R. D., and Zaveri, R. A.: A physically based estimate of radiative forcing by anthropogenic sulfate aerosol, *J. Geophys. Res.-Atmos.*, 106, 5279–5293, 2001.
- Ghan, S. J., Liu, X., Easter, R. C., Zaveri, R., Rash, P. J., and Yoon, J.-H.: Toward a minimal representation of aerosols in climate models: Comparative decomposition of aerosol direct, semi-direct and indirect radiative forcing, *J. Climate*, in press, 2012.
- Heintzenberg, J., Covert, D. C., and Van Dingenen, R.: Size distribution and chemical composition of marine aerosols: a compilation and review, *Tellus B*, 52, 1104–1122, 2000.
- Herzog, M., Weisenstein, D. K., and Penner, J. E.: A dynamic aerosol module for global chemical transport models: Model description, *J. Geophys. Res.-Atmos.*, 109, D18202, doi:10.1029/2003jd004405, 2004.
- Hoose, C., Lohmann, U., Erdin, R., and Tegen, I.: The global influence of dust mineralogical composition on heterogeneous ice nucleation in mixed-phase clouds, *Environ. Res. Lett.*, 3, 025003, doi:10.1088/1748-9326/3/2/025003, 2008.
- Howell, S. G., Clarke, A. D., Shinzuka, Y., Kapustin, V., McNaughton, C. S., Huebert, B. J., Doherty, S. J., and Anderson, T. L.: Influence of relative humidity upon pollution and dust during ACE-Asia: Size distributions and implications for optical properties, *J. Geophys. Res.*, 111, D06205, doi:10.1029/2004jd005759, 2006.
- Jacobson, M. Z.: Strong radiative heating due to the mixing state of black carbon in atmospheric aerosols, *Nature*, 409, 695–697, 2001.
- Jacobson, M. Z.: Reply to comment by J. Feichter et al. on “Control of fossil-fuel particulate black carbon and organic matter, possibly the most effective method of slowing global warming”, *J. Geophys. Res.*, 108, 4768, doi:10.1029/2002JD003299, 2003.
- Jensen, E. J., Lawson, P., Baker, B., Pilon, B., Mo, Q., Heymsfield, A. J., Bansemmer, A., Bui, T. P., McGill, M., Hlavka, D., Heymsfield, G., Platnick, S., Arnold, G. T., and Tanelli, S.: On the importance of small ice crystals in tropical anvil cirrus, *Atmos. Chem. Phys.*, 9, 5519–5537, doi:10.5194/acp-9-5519-2009, 2009.
- Jimenez, J. L., Canagaratna, M. R., Donahue, N. M., Prevot, A. S., Zhang, Q., Kroll, J. H., DeCarlo, P. F., Allan, J. D., Coe, H., Ng, N. L., Aiken, A. C., Docherty, K. S., Ulbrich, I. M., Grieshop, A. P., Robinson, A. L., Duplissy, J., Smith, J. D., Wilson, K. R., Lanz, V. A., Hueglin, C., Sun, Y. L., Tian, J., Laaksonen, A., Raatikainen, T., Rautiainen, J., Vaattovaara, P., Ehn, M., Kulmala, M., Tomlinson, J. M., Collins, D. R., Cubison, M. J., Dunlea, E. J., Huffman, J. A., Onasch, T. B., Alfarra, M. R., Williams, P. I., Bower, K., Kondo, Y., Schneider, J., Drewnick, F., Borrmann, S., Weimer, S., Demerjian, K., Salcedo, D., Cottrell, L., Griffin, R., Takami, A., Miyoshi, T., Hatakeyama, S., Shimojo, A., Sun, J. Y., Zhang, Y. M., Dzepina, K., Kimmel, J. R., Sueper, D., Jayne, J. T., Herndon, S. C., Trimborn, A. M., Williams, L. R., Wood, E. C., Middlebrook, A. M., Kolb, C. E., Baltensperger, U., and Worsnop, D. R.: Evolution of Organic Aerosols in the Atmosphere, *Science*, 326, 1525–1529, 2009.
- Johnson, K. S., Zuberi, B., Molina, L. T., Molina, M. J., Iedema, M. J., Cowin, J. P., Gaspar, D. J., Wang, C., and Laskin, A.: Processing of soot in an urban environment: case study from the Mexico City Metropolitan Area, *Atmos. Chem. Phys.*, 5, 3033–3043, doi:10.5194/acp-5-3033-2005, 2005.

- Kanakidou, M., Seinfeld, J. H., Pandis, S. N., Barnes, I., Dentener, F. J., Facchini, M. C., Van Dingenen, R., Ervens, B., Nenes, A., Nielsen, C. J., Swietlicki, E., Putaud, J. P., Balkanski, Y., Fuzzi, S., Horth, J., Moortgat, G. K., Winterhalter, R., Myhre, C. E. L., Tsigaridis, K., Vignati, E., Stephanou, E. G., and Wilson, J.: Organic aerosol and global climate modelling: a review, *Atmos. Chem. Phys.*, 5, 1053–1123, doi:10.5194/acp-5-1053-2005, 2005.
- Kinne, S., Schulz, M., Textor, C., Guibert, S., Balkanski, Y., Bauer, S. E., Bernsten, T., Berglen, T. F., Boucher, O., Chin, M., Collins, W., Dentener, F., Diehl, T., Easter, R., Feichter, J., Fillmore, D., Ghan, S., Ginoux, P., Gong, S., Grini, A., Hendricks, J., Herzog, M., Horowitz, L., Isaksen, I., Iversen, T., Kirkevåg, A., Kloster, S., Koch, D., Kristjansson, J. E., Krol, M., Lauer, A., Lamarque, J. F., Lesins, G., Liu, X., Lohmann, U., Montanaro, V., Myhre, G., Penner, J., Pitari, G., Reddy, S., Seland, O., Stier, P., Takemura, T., and Tie, X.: An AeroCom initial assessment – optical properties in aerosol component modules of global models, *Atmos. Chem. Phys.*, 6, 1815–1834, doi:10.5194/acp-6-1815-2006, 2006.
- Kirkevåg, A., Iversen, T., Seland, O., Debernard, J. B., Storelvmo, T., and Kristjansson, J. E.: Aerosol-cloud-climate interactions in the climate model CAM-Oslo, *Tellus A*, 60, 492–512, doi:10.1111/J.1600-0870.2008.00313, 2008.
- Koch, D., Schulz, M., Kinne, S., McNaughton, C., Spackman, J. R., Balkanski, Y., Bauer, S., Bernsten, T., Bond, T. C., Boucher, O., Chin, M., Clarke, A., De Luca, N., Dentener, F., Diehl, T., Dubovik, O., Easter, R., Fahey, D. W., Feichter, J., Fillmore, D., Freitag, S., Ghan, S., Ginoux, P., Gong, S., Horowitz, L., Iversen, T., Kirkevåg, A., Klimont, Z., Kondo, Y., Krol, M., Liu, X., Miller, R., Montanaro, V., Moteki, N., Myhre, G., Penner, J. E., Perlwitz, J., Pitari, G., Reddy, S., Sahu, L., Sakamoto, H., Schuster, G., Schwarz, J. P., Seland, Ø., Stier, P., Takegawa, N., Takemura, T., Textor, C., van Aardenne, J. A., and Zhao, Y.: Evaluation of black carbon estimations in global aerosol models, *Atmos. Chem. Phys.*, 9, 9001–9026, doi:10.5194/acp-9-9001-2009, 2009.
- Koretsky, C., Sverjensky, D., Salisbury, J., and D’Aria, D.: Detection of surface hydroxyl species on quartz, gamma-alumina and feldspars using diffuse reflectance infrared spectroscopy, *Geochim. Cosmochim. Acta*, 61, 2193–2210, 1997.
- Kumar, P., Nenes, A., and Sokolik, I.: The importance of adsorption for CCN activity and hygroscopic properties of mineral dust aerosol, *Geophys. Res. Lett.*, 36, L24804, doi:10.1029/2009GL040827, 2009.
- Lawson, R. P., Baker, B. A., Pilon, B., and Mo, Q.: In situ observations of the microphysical properties of wave, cirrus and anvil clouds, Part 2: Cirrus cloud, *J. Atmos. Sci.*, 63, 3186–3203, 2006.
- Liousse, C., Penner, J. E., Chuang, C., Walton, J. J., Eddleman, H., and Cachier, H.: A global three-dimensional model study of carbonaceous aerosols, *J. Geophys. Res.*, 101, 19411–19432, 1996.
- Liu, X. H., Penner, J. E., and Herzog, M.: Global modeling of aerosol dynamics: Model description, evaluation, and interactions between sulfate and nonsulfate aerosols, *J. Geophys. Res.-Atmos.*, 110, D18206, doi:10.1029/2004jd005674, 2005.
- Liu, X. H., Penner, J. E., Das, B., Bergmann, D., Rodriguez, J. M., Strahan, S., Wang, M., and Feng, Y.: Uncertainties in global aerosol simulations: Assessment using three meteorological datasets, *J. Geophys. Res.*, 112, D11212, doi:10.1029/2006JD008216, 2007.
- Lohmann, U. and Feichter, J.: Global indirect aerosol effects: a review, *Atmos. Chem. Phys.*, 5, 715–737, doi:10.5194/acp-5-715-2005, 2005.
- Mahowald, N., Engelstaedter, S., Luo, C., Sealy, A., Artaxo, P., Benitez-Nelson, C., Bonnet, S., Chen, Y., Chuang, P. Y., Cohen, D. D., Dulac, F., Herut, B., Johansen, A. M., Kubilay, N., Losno, R., Maenhaut, W., Paytan, A., Prospero, J. M., Shank, L. M., and Siefert, R. L.: Atmospheric Iron deposition: Global distribution, variability and human perturbations, *Ann. Rev. Mar. Sci.*, 1, 245–278, doi:10.1146/annurev.marine.010908.163727, 2009.
- McFarquhar, G. M., Um, J., Freer, M., Baumgardner, D., Kok, G. L., and Mace, G.: Importance of small ice crystals to cirrus properties: Observations from the Tropical Warm Pool International Cloud Experiment (TWP-ICE), *Geophys. Res. Lett.*, 34, L13803, doi:10.1029/2007gl029865, 2007.
- McGraw, R.: Description of aerosol dynamics by the quadrature method of moments, *Aerosol Sci. Technol.*, 27, 255–265, 1997.
- McNaughton, C. S., Clarke, A. D., Kapustin, V., Shinzuka, Y., Howell, S. G., Anderson, B. E., Winstead, E., Dibb, J., Scheuer, E., Cohen, R. C., Wooldridge, P., Perring, A., Huey, L. G., Kim, S., Jimenez, J. L., Dunlea, E. J., DeCarlo, P. F., Wennberg, P. O., Crouse, J. D., Weinheimer, A. J., and Flocke, F.: Observations of heterogeneous reactions between Asian pollution and mineral dust over the Eastern North Pacific during INTEX-B, *Atmos. Chem. Phys.*, 9, 8283–8308, doi:10.5194/acp-9-8283-2009, 2009.
- Merrill, J. T., Uematsu, M., and Bleck, R.: Meteorological Analysis of Long Range Transport of Mineral Aerosols Over the North Pacific, *J. Geophys. Res.*, 94, 8584–8598, doi:10.1029/JD094iD06p08584, 1989.
- Minikin, A., Petzold, A., Strom, J., Krejci, R., Seifert, M., van Velthoven, P., Schlager, H., and Schumann, U.: Aircraft observations of the upper tropospheric fine particle aerosol in the Northern and Southern Hemispheres at midlatitudes, *Geophys. Res. Lett.*, 30, 1503, doi:10.1029/2002gl016458, 2003.
- Moffet, R. C. and Prather, K. A.: In-situ measurements of the mixing state and optical properties of soot with implications for radiative forcing estimates, *P. Natl. Acad. Sci. USA*, 2062, 11872–11877, doi:10.1073/Pnas.0900040106, 2009.
- Monahan, E., Spiel, D. E., and Davidson, K. L.: A model of marine aerosol generation via whitecaps and wave disruption, in: *Oceanic Whitecaps*, edited by: Monahan, E. C. and Mac-Niochail, G., Norwell, Mass, D. Reidel, 167–193, 1986.
- Moteki, N. and Kondo, Y.: Effects of mixing state on black carbon measurements by laser-induced incandescence, *Aerosol Sci. Technol.*, 41, 398–417, doi:10.1080/02786820701199728, 2007.
- Moteki, N., Kondo, Y., Miyazaki, Y., Takegawa, N., Komazaki, Y., Kurata, G., Shirai, T., Blake, D. R., Miyakawa, T., and Koike, M.: Evolution of mixing state of black carbon particles: Aircraft measurements over the western Pacific in March 2004, *Geophys. Res. Lett.*, 34, L11803, doi:10.1029/2006gl028943, 2007.
- Pierce, J. R. and Adams, P. J.: Global evaluation of CCN formation by direct emission of sea salt and growth of ultrafine sea salt, *J. Geophys. Res.*, 111, D06203, doi:10.1029/2005JD006186, 2006.
- Posfai, M., Simonics, R., Li, J., Hobbs, P. V., and Buseck, P. R.: Individual aerosol particles from biomass burning in southern Africa: 1. Compositions and size distributions of carbonaceous particles, *J. Geophys. Res.*, 108, 8483–8496, 2003.

- Pratt, K. A. and Prather, K. A.: Aircraft measurements of vertical profiles of aerosol mixing states, *J. Geophys. Res.*, 115, D11305, doi:10.1029/2009JD013150, 2010.
- Prospero, J. M., Uematsu, M., and Savoie, D. L.: Mineral aerosol transport to the Pacific Ocean, in: *Chemical Oceanography*, edited by: Ridley, J. P., Chester, R., and Duce, R. A., Elsevier, New York, 188–218, 1989.
- Riemer, N., West, M., Zaveri, R. A., and Easter, R. C.: Simulating the evolution of soot mixing state with a particle-resolved aerosol model, *J. Geophys. Res.-Atmos.*, 114, D09202, doi:10.1029/2008jd011073, 2009.
- Savoie, D. L., Prospero, J. M., Larsen, R. J., Huang, F., Izaguirre, M. A., Huang, T., Snowdon, T. H., Custals, L., and Sanderson, C. G.: Nitrogen and Sulfur Species in Antarctic Aerosols at Mawson, Palmer Station, and Marsh (King George Island), *J. Atmos. Chem.*, 17, 95–122, 1993.
- Savoie, D. L., Prospero, J. M., and Saltzman, E. S.: Nitrate, non-seasalt sulfate and methanesulfonate over the Pacific Ocean, in: *Chemical Oceanography*, edited by: Ridley, J. P., Chester, R., and Duce, R. A., Elsevier, New York, 219–250, 1989.
- Schwarz, J. P., Gao, R. S., Fahey, D. W., Thomson, D. S., Watts, L. A., Wilson, J. C., Reeves, J. M., Darbeheshti, M., Baumgardner, D. G., Kok, G. L., Chung, S. H., Schulz, M., Hendricks, J., Lauer, A., Kaercher, B., Slowik, J. G., Rosenlof, K. H., Thompson, T. L., Langford, A. O., Loewenstein, M., and Aikin, K. C.: Single-particle measurements of midlatitude black carbon and light-scattering aerosols from the boundary layer to the lower stratosphere, *J. Geophys. Res.*, 111, D16207, doi:10.1029/2006jd007076, 2006.
- Schwarz, J. P., Spackman, J. R., Gao, R. S., Watts, L. A., Stier, P., Schulz, M., Davis, S. M., Wofsy, S. C., and Fahey, D. W.: Global-scale black carbon profiles observed in the remote atmosphere and compared to models, *Geophys. Res. Lett.*, 37, L18812, doi:10.1029/2010GL044372, 2010.
- Seland, O., Iversen, T., Kirkevåg, A., and Storelvmo, T.: Aerosol-climate interactions in the CAM-Oslo atmospheric GCM and investigation of associated basic shortcomings, *Tellus A*, 60, 459–491, doi:10.1111/j.1600-0870.2008.00318.x, 2008.
- Seinfeld, J. H. and Pandis, S. N.: *Atmospheric Chemistry and Physics: From Air Pollution to Climate Change*, Hoboken, N. J, John Wiley, 1998.
- Shinozuka, Y., Clarke, A. D., Howell, S. G., Kapustin, V. N., McNaughton, C. S., Zhou, J. C., and Anderson, B. E.: Aircraft profiles of aerosol microphysics and optical properties over North America: Aerosol optical depth and its association with PM<sub>2.5</sub> and water uptake, *J. Geophys. Res.*, 112, D12S20, doi:10.1029/2006jd007918, 2007.
- Sokolik, I. N. and Toon, O. B.: Direct radiative forcing by anthropogenic airborne mineral aerosols, *Nature* 381, 681–683, 1996.
- Spracklen, D. V., Pringle, K. J., Carslaw, K. S., Chipperfield, M. P., and Mann, G. W.: A global off-line model of size-resolved aerosol microphysics: I. Model development and prediction of aerosol properties, *Atmos. Chem. Phys.*, 5, 2227–2252, doi:10.5194/acp-5-2227-2005, 2005.
- Stevens, B. and Feingold, G.: Untangling aerosol effects on clouds and precipitation in a buffered system, *Nature*, 461, 607–613, doi:10.1038/nature08281, 2009.
- Stier, P., Feichter, J., Kinne, S., Kloster, S., Vignati, E., Wilson, J., Ganzeveld, L., Tegen, I., Werner, M., Balkanski, Y., Schulz, M., Boucher, O., Minikin, A., and Petzold, A.: The aerosol-climate model ECHAM5-HAM, *Atmos. Chem. Phys.*, 5, 1125–1156, doi:10.5194/acp-5-1125-2005, 2005.
- Textor, C., Schulz, M., Guibert, S., Kinne, S., Balkanski, Y., Bauer, S., Bernsten, T., Berglen, T., Boucher, O., Chin, M., Dentener, F., Diehl, T., Easter, R., Feichter, H., Fillmore, D., Ghan, S., Ginoux, P., Gong, S., Grini, A., Hendricks, J., Horowitz, L., Huang, P., Isaksen, I., Iversen, I., Kloster, S., Koch, D., Kirkevåg, A., Kristjansson, J. E., Krol, M., Lauer, A., Lamarque, J. F., Liu, X., Montanaro, V., Myhre, G., Penner, J., Pitari, G., Reddy, S., Seland, Ø., Stier, P., Takemura, T., and Tie, X.: Analysis and quantification of the diversities of aerosol life cycles within AeroCom, *Atmos. Chem. Phys.*, 6, 1777–1813, doi:10.5194/acp-6-1777-2006, 2006.
- Vignati, E., Wilson, J., and Stier, P.: M7: An efficient size-resolved aerosol microphysics module for large-scale aerosol transport models, *J. Geophys. Res.-Atmos.*, 109, D22202, doi:10.1029/2003jd004485, 2004.
- Wang, J., Cubison, M. J., Aiken, A. C., Jimenez, J. L., and Collins, D. R.: The importance of aerosol mixing state and size-resolved composition on CCN concentration and the variation of the importance with atmospheric aging of aerosols, *Atmos. Chem. Phys.*, 10, 7267–7283, doi:10.5194/acp-10-7267-2010, 2010.
- Wang, M. H., Penner, J. E., and Liu, X. H.: Coupled IMPACT aerosol and NCAR CAM3 model: Evaluation of predicted aerosol number and size distribution, *J. Geophys. Res.-Atmos.*, 114, D06302, doi:10.1029/2008jd010459, 2009.
- Wang, M. H., Ghan, S., Easter, R., Ovchinnikov, M., Liu, X., Kasianov, E., Qian, Y., Gustafson Jr., W. I., Larson, V. E., Schanen, D. P., Khairoutdinov, M., and Morrison, H.: The multi-scale aerosol-climate model PNNL-MMF: model description and evaluation, *Geosci. Model Dev.*, 4, 137–168, doi:10.5194/gmd-4-137-2011, 2011.
- Whitby, E. and McMurry, P.: Modal aerosol dynamics modelling, *Aerosol Sci. Tech.*, 27, 673–688, 1997.
- Wilson, J., Cuvelier, C., and Raes, F.: A modeling study of global mixed aerosol fields, *J. Geophys. Res.-Atmos.*, 106, 34081–34108, 2001.
- Wright, D. L., Kasibhatla, P. S., McGraw, R., and Schwartz, S. E.: Description and evaluation of a six-moment aerosol microphysical module for use in atmospheric chemical transport models, *J. Geophys. Res.-Atmos.*, 106, 20275–20291, 2001.
- Yoon, C. and McGraw, R.: Representation of generally mixed multivariate aerosols by the quadrature method of moments: II. Aerosol dynamics, *J. Aerosol Sci.*, 35, 577–598, doi:10.1016/J.Jaerosci.2003.11.012, 2004.
- Zaveri, R. A., Easter, R. C., Fast, J. D., and Peters, L. K.: Model for Simulating Aerosol Interactions and Chemistry (MOSAIC), *J. Geophys. Res.*, 113, D13204, doi:10.1029/2007JD008782, 2008.
- Zaveri, R. A., Easter, R. C., Barnard, J. C., Riemer, N., and West, M.: Particle-resolved simulation of aerosol size, composition, mixing state, and the associated optical and cloud condensation nuclei activation properties in an evolving urban plume, *J. Geophys. Res.-Atmos.*, 115, D17210, doi:10.1029/2009JD013616, 2010.
- Zhang, M. H., Lin, W. Y., Bretherton, C. S., Hack, J. J., and Rasch, P. J.: A modified formulation of fractional stratiform condensation rate in the NCAR Community Atmospheric Model (CAM2), *J. Geophys. Res.-Atmos.*, 108, 4035, doi:10.1029/2002jd002523,

- 2003.
- Zhang, Q., Jimenez, J. L., Canagaratna, M. R., Allan, J. D., Coe, H., Ulbrich, I., Alfarra, M. R., Takami, A., Middlebrook, A. M., Sun, Y. L., Dzepina, K., Dunlea, E., Docherty, K., DeCarlo, P. F., Salcedo, D., Onasch, T., Jayne, J. T., Miyoshi, T., Shimojo, T., Hatakeyama, S., Takegawa, N., Kondo, Y., Schneider, J., Drewnick, F., Borrmann, S., Weimer, S., Demerjian, K., Williams, P., Bower, K., Bahreini, R., Cottrell, L., Griffin, R. J., Rautiainen, J., Sun, J. Y., Zhang, Y. M., and Worsnop, D. R.: Ubiquity and dominance of oxygenated species inorganic aerosols in anthropogenically-influenced Northern Hemisphere midlatitudes, *Geophys. Res. Lett.*, 34, L13801, doi:10.1029/2007GL029979, 2007.
- Zhang, Y., Easter, R. C., Ghan, S. J., and Abdul-Razzak, H.: Impact of aerosol size representation on modeling aerosol-cloud interactions, *J. Geophys. Res.-Atmos.*, 107, 4558, doi:10.1029/2001jd001549, 2002.